PAPER

Check for updates

Multifunctional erythromycin-loaded liposomes: a methodological optimization for enhanced mucoadhesion, antioxidant activity, and biocompatibility

Vera-Maria Platon,[a] Anda Mihaela Craciun,[a] Irina Rosca, [iD][a] Natalia Simionescu [iD][a] and Luminita Marin [iD] *[a,b]

In recent years, liposomes have emerged as versatile nanocarriers for the delivery of antibacterial agents, enhancing drug pharmacokinetics in an effort to overcome antibiotic resistance. This study presents a systematic, multivariate optimization of erythromycin-loaded liposomes (ERY-liposomes) coated with chitosan oligomers (CSO), aiming for drug encapsulation into nanoscale-sized particles, while promoting mucoadhesive, antioxidant, antimicrobial, and biocompatibility attributes. Critical formulation parameters including lipid-to-drug ratio, thin-film formation conditions, hydration medium and time, liposome down-sizing technique, chitosan molecular weight and concentration, as well as cryoprotectant content were comprehensively optimized via multivariate analysis. Physicochemical and structural characterization was conducted using a broad array of techniques: FTIR, ^{1}H-NMR, DLS, STEM, AFM, XRD, and variable temperature polarized light microscopy (POM). The optimized ERY-liposomes achieved an encapsulation efficiency of 63%, a hydrodynamic diameter of 97 nm, and a low polydispersity index (PDI < 0.1), indicative of uniform size distribution. Structural analysis revealed strong intermolecular forces among ERY, CSO and the phospholipid, resulting in densely packed vesicles incorporating the drug in an amorphous state. STEM imaging displayed spherical morphology with compact cores surrounded by a rough coating, and POM indicated enhanced thermal stability. The formulation demonstrated sustained ERY release governed by diffusion and matrix erosion mechanisms, potent antibacterial activity over 24 hours, and considerable early bactericidal activity, particularly against Gram-positive strains. Additionally, ERY-liposomes displayed pronounced scavenging activity (80% radical inhibition, EC_{50} = 0.396 mg mL^{-1} ERY), and mucoadhesive properties, as well as cytocompatibility with normal human fibroblasts. These findings indicate the advanced therapeutic potential of ERY-liposomes.

1. Introduction

Erythromycin (ERY), a macrolide antibiotic derived from *Saccharopolyspora erythraea*, remains an important therapeutic agent with broad-spectrum antibacterial activity. It is widely prescribed for treating infections of the respiratory tract, skin and soft tissues, gastrointestinal and urogenital systems, ocular conditions, and is also employed in endocarditis prophylaxis in penicillin-allergic patients undergoing dental or surgical procedures, as well as in the prevention of neonatal ophthalmia and management of myotonic dystrophy symptoms.[1–6] These diverse applications are supported not only by ERY's antibacterial efficacy, primarily against Gram-positive pathogens, but also by its immunomodulatory properties, which contribute to its role in treating chronic inflammatory conditions.[6,7]

Despite its clinical relevance, erythromycin exhibits a number of pharmaceutical and biological limitations that hinder its optimal therapeutic use. These include poor water solubility, instability in acidic media, and short plasma half-life, necessitating frequent dosing that impacts patient compliance and raises the risk of adverse effects such as hepatotoxicity and cardiotoxicity.[5,8] ERY is also sensitive to oxidation and light, requiring careful storage conditions.[9] Moreover, its limited ability to penetrate biofilms, as well as its numerous side effects upon systemic administration, represent further impediments to achieving treatment efficiency. Most critically, the extensive clinical and food animal production use of ERY has accelerated the emergence of bacterial resistance, reduced

[a]*"Petru Poni" Institute of Macromolecular Chemistry, Aleea Gr. Ghica Voda 41A, Iasi 700487, Romania. E-mail: lmarin@icmpp.ro*
[b]*"Alexandru Ioan Cuza" University, Faculty of Chemistry, Bd. Carol I nr. 11, 700506 Iasi, Romania*

its effectiveness and augmented the urgency for innovative solutions.[5,10–13]

Driven by the need to overcome the limitations of ERY, researchers increasingly focused on encapsulating it within formulations of diverse chemical compositions, sizes, and morphologies. This led to the development of a wide range of (nano)formulations, including various vesicles (liposomes, niosomes, micelles, solid lipid particles, ethosomes, cubosomes), micro(nano)spheres, cyclodextrin complexes, gels, (nano) fibers, mesoporous oxides, and metallic nanoparticles.[5] Among them, liposomes have gained considerable attention as a promising drug delivery platform, offering solutions to several limitations of conventional therapies, *i.e.* low bioavailability, rapid clearance from circulation, limited target specificity, uncontrolled drug release, and the emergence of drug resistance.[14–16]

Liposomes are spherical vesicles composed of phospholipid bilayers capable of encapsulating both hydrophilic and hydrophobic drugs. Their ability to enhance solubility, protect labile compounds from degradation and clearance, while providing sustained and targeted release makes them particularly suitable for antibiotics like erythromycin.[17–19] Furthermore, liposomal encapsulation can reduce systemic toxicity, improve bioavailability, and enhance cellular uptake, potentially overcoming microbial resistance mechanisms.[15,20]

In silico analyses and preclinical data suggest that erythromycin-loaded liposomes offer one of the most promising macrolide formulations for future applications.[21] However, no systematic methodology has yet been established for preparing ERY liposomes with an optimal balance between encapsulation efficiency, nanoparticle size, and functional biological properties.[5] To this end, a rational design approach is needed to develop scalable, reproducible formulations tailored to overcome the drawbacks of erythromycin.

Surface modification of liposomes with biocompatible polymers presents a compelling strategy to further enhance their therapeutic performance. Among the available polymers, chitosan, a naturally derived, biodegradable, and biocompatible polysaccharide, stands out for its mucoadhesive, antibacterial, and antioxidant properties. The cationic nature of chitosan allows it to interact electrostatically with the negatively charged surface of liposomes, improving colloidal stability, preventing liposome aggregation, and facilitating enhanced cellular uptake through endocytosis.[22–25] Moreover, chitosan oligomers which have improved aqueous solubility, biological activity, and mucosal permeability compared to chitosan, keep the promise to mitigate the risk of liposome bridging.[26] Chitosan coating not only enhances mucoadhesion and local drug availability at epithelial and mucosal surfaces (*e.g.*, ocular, gastric, pulmonary, and wound tissues) but may also modulate tight junctions, promoting paracellular drug transport and improving intracellular ERY delivery. Additionally, chitosan may contribute to the antioxidant defence, which is highly beneficial in reducing oxidative stress at infection or inflammation sites, protecting both the drug and the host tissues.[27] This is particularly advantageous in therapies targeting sensitive tissues such as those of the eye, gastrointestinal tract, or lungs, where local inflammation and oxidative damage may compromise therapeutic success.

Therefore, the present study aims to develop a robust, scalable, and reproducible methodology for formulating erythromycin-loaded liposomes coated with chitosan oligomers, optimized through a systematic investigation of formulation parameters. By tailoring the composition, preparation method, and CSO coating conditions, this study seeks to produce a nanocarrier system with superior stability, antioxidant potential, mucoadhesive properties, and antibacterial efficacy, ultimately addressing the limitations of conventional erythromycin therapy.

2. Materials and methods

2.1. Materials

Erythromycin (potency ≥850 µg per mg), L-α-phosphatidylcholine (PC) from egg yolk, sucrose (SUC), 2,2-diphenyl-1-picrylhydrazyl (DPPH), lysozyme from chicken egg white (protein ≥90%, ≥40 000 units per mg protein), lipase (from *Candida antarctica*, lyophilized, powder, beige, 0.4 U mg^{-1}), dialysis tubing cellulose membrane (33 mm × 21 mm, molecular weight cut-off = 14 000), sodium dihydrogen phosphate monohydrate, disodium hydrogen phosphate, sodium chloride, potassium chloride, sodium hydroxide (95%), methanol, chloroform (CHCl$_3$) (for spectroscopy Uvasol®) and acetic acid (98.9%) were purchased from Sigma Aldrich and used as received. Ethanol (98.89%) was purchased from Sigma Aldrich and subjected to drying on molecular sieves before use. Sulfuric acid (95.0–97.0%, ACS Reagent Grade) was purchased from Honeywell. Chitosan (M_w = 302 kDa, DD = 82%) was acquired from Sigma Aldrich, and subjected to alkaline hydrolysis in order to obtain chitosan with lower molecular weight (M_w = 126 kDa, DD = 97%). Chitosan oligomers with a polymerization degree of approximately 10 and deacetylation degree (DD) of 82%, were prepared by nitrous depolymerization of chitosan (147 kDa, DD = 82%) acquired from Sigma Aldrich.[28,29] Phosphate buffer solution (PBS) of pH 7.4 has been prepared in our laboratory following a well-established procedure.[30]

2.2. Preparation of vesicles

The liposomes were prepared using the thin-film hydration method. After many trials aiming to optimize a technique to attain liposomes with low size and narrow dispersity, (Tables S1–S7 and Fig. S1–S4) the optimal one was found to be the following. A lipid film was prepared by adding ERY and PC in a 1 : 6 mass ratio (2.5 mg ERY, 15 mg PC) into a 50 mL round bottom flask and dissolving the components in 10 mL CHCl$_3$ in order to obtain an ERY concentration of 0.25 mg mL^{-1}. The solvent was removed by rotary evaporation at 45 °C, after which the flask was left to dry in an enclosed space (chemical hood), in order to eliminate any residual chloroform traces. Then, the dried thin film was hydrated by adding 1 mL of PBS 7.4 under slight temperature (37 °C) and vigorous magnetic stirring (1100 rpm) over the course of 60 hours in order to

ensure homogeneity. The obtained suspension was extruded by passing 21 times through polycarbonate membranes with a 100 nm pore size on a heating block, previously heated to 37 °C. Following the extrusion process, the suspension was added drop-wise to a 0.5% CSO solution in 0.5% acetic acid, under stirring (120 rpm) for approximately 30 minutes, in order to coat the vesicles (liposome suspension/CSO solution = 1/1, v/v). Upon completion of the coating process, a 400 mM sucrose solution was added to the mixture, under stirring for 30 minutes, to reach a volumetric ratio between liposome suspension, CSO solution and sucrose solution of 1 : 1 : 1. The final CSO-coated ERY-liposomal suspension was subjected to dialysis in order to remove any free drug, as well as any traces of acetic acid used in the preparation process. Dialysis was performed using cellulose membranes and a washing medium identical to that of the liposome medium, namely a mixture of sucrose solution, PBS 7.4, and ultrapure water in the same ratio as in the samples, to ensure the stability of their composition. The washing step was carried out under gentle stirring over an ice bath, monitoring the pH and replacing the medium with fresh one multiple times until neutral pH = 7 was attained.

Plain ERY-liposomes (EL), as well as plain coated liposomes (CL) were both prepared as control samples. The samples' compositions and codes can be found in Table 1.

2.3. Equipment and methods

2.3.1. Extrusion. Extrusion was performed using a miniextruder equipped with two 1 mL gas-tight syringes and a heating block (Avanti®), Polyester Drain Discs – 10 mm (Whatman®) and polycarbonate membranes with 100 nm pores (Avanti®).

2.3.2. Freeze drying. Freeze drying was performed using a LABCONCO FreeZone Freeze Dry System (Kansas, MO, USA), for 24 h, 1.510 mbar and −54 °C.

2.3.3. FTIR. Fourier-transform infrared (FTIR) spectra were registered on a FT-IR IRAffinity-1S (Shimadzu, Kyoto, Japan), freeze-drying the liposomal suspension and placing it on potassium bromide supports. The spectra were recorded between 4000–400 cm^{-1}, with 32 scans, using a resolution of 4 cm^{-1}. Spectral deconvolution was carried out using the second derivative function, followed by curve fitting performed with the OPUS 6.5 and OriginPro software. Peak areas were calculated using a 50% Lorentzian and 50% Gaussian mixed function. The Root Mean Squared Error (RMSE) was <0.005 for all spectra.

2.3.4. H-NMR. Proton nuclear magnetic resonance (^{1}H-NMR) spectra were registered on a Bruker Avance NEO 400 MHz NMR apparatus (Bruker Biospin, Ettlingen, Germany). Samples were prepared by freeze-drying the liposomal suspension and later dissolving it in a mixture of MeOD and a 1.33% HCl solution in D$_2$O in a 1 : 4 ratio (v/v).

2.3.5. XRD. Wide angle X-ray diffraction (XRD) of the liposomes was performed via a Benchtop Miniflex 600 Rigaku diffractometer (Tokyo, Japan), in the range of 2–50 °C, 3 °C per minute and 0.0025 step. Samples were also prepared by previous freeze-drying.

2.3.6. STEM. Scanning transmission electron microscopy (STEM) images were obtained on a Verios G4 UC (Thermo Fischer Scientific) scanning transmission electronic microscope, operated at 5 kV acceleration voltage. After proper dilution with ultrapure water, the suspensions were placed on copper grids, dried, and then subjected to STEM analysis. The ImageJ program was used to assess the average diameter of the liposomes.

2.3.7. POM. Variable temperature polarized light microscopy (POM) images were obtained via a Zeiss Axio Imager M2 microscope.

2.3.8. AFM. Atomic force microscopy (AFM) measurements were performed on a commercial AFM NTMDT atomic force microscope. The images were taken in the tapping mode with typical resonance frequency of 240 kHz. Dried liposomes were supported on glass.

2.3.9. DLS. The size distribution and zeta potential of the particles was measured by DLS using a computerized Zetasizer Nano ZS (Malvern). ECL suspensions were diluted until a stable signal was obtained, and measured in triplicate.

2.3.10. Stability studies. Stability studies were carried out by placing diluted ECL samples (1 : 1 v/v) in enclosed spaces at 5, 25 and 50 °C over a period of 8 weeks and measuring their particle size by DLS.

2.3.11. UV-VIS. UV-VIS spectroscopy was performed on an Agilent Carry 60 UV-Vis spectrophotometer in order to determine the encapsulation efficiency (EE%) of ERY in the liposomes and to perform the release studies.

2.3.12. Quantification of ERY. Quantification of ERY was performed using the sulfuric acid method.[31] Liposome suspensions were reacted with equal volumes of H$_2$SO$_4$ 27 N, at 50 °C for 30 minutes, when a yellow-coloured solution with an absorption maximum at 482 nm is formed. Prior to quantification, a calibration curve was obtained, using ERY solutions in PBS 7.4, with concentrations ranging from 5 to 100 μg mL^{-1}, graphically representing their absorbance as a function of concentration (Fig. S5). Samples were tested in triplicate. The encapsulation efficiency was calculated using the formula:

$$EE\% = (M_D/M_T) \times 100,$$

where M_D represents the amount of ERY determined in the sample after removal of free drug, and M_T represents the total amount of drug added initially.

2.3.13. *In vitro* release kinetics. The *in vitro* release kinetics of ERY was assessed by immersing 1 mL of liposomal suspension (containing 1.55 ± 0.065 mg ERY) into 10 mL PBS of physiological pH (pH = 7.4) supplemented with lipase (100 U L^{-1}) and lysozyme (376 U L^{-1}).[32,33] Dialysis membranes were used to immerse the suspension, placing the samples in an incubator at 37 °C and 25 rpm. At certain periods of time (from 15 to 2880 minutes), 1 mL

Table 1 Amount of each component used in liposome preparation

	ERY (mg)	PC (mg)	CSO (mg)	Sucrose (mg)
ECL	2.5	15	5	136.8
CL	—	15	5	136.8
EL	2.5	15	—	136.8

aliquots were withdrawn from the release media of each sample and replaced with fresh one. The absorbances of the aliquots were measured by UV-Vis spectroscopy, employing the H_2SO_4 method previously described, at the specific wavelength of 482 nm. The addition of standard method was implied, when the UV signal of ERY was beneath the detection limit. In this case, standard ERY solution was added to the aliquots, and the standard's absorbance was subtracted from the overall absorbance. The values were fitted on a previously generated calibration curve, by reading the absorbances of ERY solutions with well-known concentrations and graphically representing them as a function of concentration (Fig. S5). Samples were tested in triplicate.

The mechanism of drug release was assessed by fitting the *in vitro* release data to the mathematical equations of the following models:

Zero order model: $Q_t = K_0 \times t$, where K_0 is the zero order release constant and Q_t is the amount of drug dissolved in time t.

First order model: $\log Q_t = K \times t/2.303$, where K is the first order release constant and Q_t is the quantity of drug released in time t.

Higuchi model: $Q_t = K_H \times t^{\frac{1}{2}}$, where K_H is the Higuchi dissolving constant and Q_t is the quantity of drug released in time t.

Korsmeyer–Peppas model: is expressed as follows: $M_t/M_\infty = K \times t^n$, where n is the release exponent, K is the release rate constant, and M_t/M_∞ is the fraction of drug released at time t. The model was applied up to 60% drug release, eliminating the burst release stage.

Hixson–Crowell model: $W_0^{1/3} - W_t^{1/3} = K \times t$, where W_0 is the initial amount of drug in the pharmaceutical dosage form, W_t is the remaining amount of drug in the pharmaceutical dosage form time t and K is a constant.

2.3.14. Antioxidant activity. Antioxidant activity was assessed using the DPPH assay. After quantifying the ERY content, the liposomal suspension was diluted with a mixture of ultrapure water and PBS (pH 7.4), consistent with the liposome formulation, to reach volumetric ratios of 1/0, 1/1, 1/3, 1/7, 1/15 v/v. A DPPH solution, 2.5 mg per 100 mL in spectroscopic-grade methanol, was prepared. Each liposomal sample was then mixed with the DPPH solution in a 1 : 1 volume ratio and incubated for 45 minutes in the absence of light, to prevent light-induced degradation of the free radicals. Absorbance was measured at 517 nm. A control sample was prepared by incubating the DPPH solution with the PBS–water mixture (1 : 1 v/v) under the same conditions. In order to assess the contribution of each component, reference solutions of ERY, PC, and CSO at concentrations equivalent to those in the undiluted liposomal suspensions were prepared and tested following the same procedure. All measurements were performed in triplicate. Antioxidant activity was calculated using the following formula:

$$\text{Scavenging activity } (\%) = (A_{\text{DPPH}} - A_{\text{sample}})/A_{\text{DPPH}} \times 100,$$

where A represents the measured absorbance of the DPPH control and of the sample, respectively.

The concentration showing 50% scavenging activity EC50 was calculated by plotting the concentration *vs.* scavenging activity.

2.3.15. Mucoadhesive properties. The *mucoadhesive properties* of the liposomes were investigated by measuring the turbidity of a mucin solution, neat liposomal suspensions and liposomal suspensions incubated with mucin, in similar conditions. The mucin solution (1 g L^{-1}) was prepared by magnetic stirring for 1 hour at room temperature, followed by filtration through disposable syringe filters (0.45 μm). After separate reading, the mucin solution and the liposomal suspensions (diluted to an equivalent of 0.3 mM PC) were mixed in a 1/1 ratio (v/v). The turbidity measurements were performed by measuring the transmittance (*T*%) at 320 nm, after prior incubation for 30 minutes.

2.3.16. Antibacterial activity. The antibacterial activity of the samples was determined by disk diffusion assay[34] against a Gram-positive bacterial strain represented by *Enterococcus faecalis* ATCC29212, and a Gram-negative bacterial strain represented by *Klebsiella pneumoniae* ATCC10031. All microorganisms were stored at −80 °C in 20% glycerol. The bacterial strains were refreshed on nutrient agar (NA) at 37 °C and the microbial suspensions were prepared with these cultures in a sterile solution, to obtain turbidity optically comparable to that of 0.5 McFarland standards. Volumes of 0.1 mL from each inoculum were spread onto NA plates and 15 μl of the samples were added on the inoculated plates. To evaluate the antimicrobial properties, the growth inhibition was measured under standard conditions after 24 hours of incubation at 37 °C.

All tests were carried out in triplicate to verify the results. After incubation, the samples were analysed with SCAN1200®, version 8.6.10.0 (Interscience) and were expressed as the mean ± standard deviation (SD) performed with GraphPad Prism software version 7.00 for Windows (GraphPad Software, La Jolla California USA, **https://www.graphpad.com**).

2.3.17. Viable cell-counting method. Viable cell-counting method which evaluates kinetics of bacterial cell growth[35] was also performed in order to quantify the antibacterial activity of the samples against the reference bacterial strains. The bacterial strains were refreshed on NA at 37 °C. Microbial suspensions were prepared with these cultures in sterile nutrient broth medium in order to obtain turbidity optically comparable to that of 0.5 McFarland standards. The samples were placed into solutions which contained 0.3 mL of the bacterium suspensions and 2.7 mL 1× PBS solution, followed by incubation in a shaker at 37 °C up to 24 hours. A control experiment was conducted. 1 μL of the control samples and of the treated samples were removed at determined periods of incubation time and spread on Plate Count Agar plates. The number of colonies was counted after 24 hours of incubation at 37 °C. All tests were carried out in triplicate to verify the results. After incubation, the plates were analysed with SCAN1200®, version 8.6.10.0 (Interscience, France) and the number of colonies was expressed as the mean ± standard deviation (SD) performed with GraphPad Prism software version 7.00 for Windows (GraphPad Software, La Jolla California USA, **https://www.graphpad.com**).

2.3.18. Cell viability assay. The cytotoxicity of studied liposomal formulations and ERY was evaluated following a standardized cytotoxicity protocol conducted by the accredited IntelCentru laboratories in "Petru Poni" Institute in accordance with DIN EN ISO 10993-5:2009,[36] which assesses the *in vitro* cytotoxic potential of medical devices, according to the manufacturer's instructions using the CellTiter-Glo® 2.0 Assay (Promega, Madison, WI, USA). Human gingival fibroblasts (HGF, CLS Cell Lines Service GmbH, Eppelheim, Germany) were grown in complete cell culture medium: αMEM medium with 10% fetal bovine serum and 1% antibiotic-antimycotic (all from Gibco, Thermo Fisher Scientific, Waltham, MA, USA). Cells were seeded into 96-well white opaque tissue culture-treated plates (50 000 cells per mL), allowed to adhere overnight, then incubated with different concentrations of samples (from 10 to 60 μg ERY per mL) for 24 h, in triplicate experiments. CL were diluted identically to ECL for comparison purposes. After 24 h incubation time, CellTiter-Glo® reagent was added, and luminescence was recorded using a FLUOstar® Omega microplate reader (BMG LABTECH, Ortenberg, Germany). Treated cells' viability was calculated as percentage of untreated cells' viability and data were represented graphically as means ± standard deviations.

3. Results and discussion

## 3.1. Rational design and optimization of ERY liposomes preparation

Erythromycin-loaded liposomes coated with chitosan oligomers (ECL) were prepared using an optimized thin-film hydration method, followed by extrusion, achieving high encapsulation efficiency, nanoscale dimensions with narrow size distribution, and enhanced stability for safe storage and application. The optimization involved a systematic variation of key parameters, including the lipid-to-drug ratio, conditions for thin-film formation (rotation speed, temperature, flask volume, and timing of erythromycin addition), hydration medium (PBS *vs.* water), hydration time, downsizing method (ultrasonication *vs.* extrusion), concentration and molecular weight of the chitosan coating, as well as concentration of stabilizing agent (sucrose) (Scheme 1, Tables S1–S7 and Fig. S1–S4).

By varying the mass ratio of PC : ERY in chloroform from 2 : 1 to 8 : 1, it was observed that a ratio of 6 : 1 resulted in liposomes with the smallest size and lowest polydispersity (Table S1). This was attributed to the optimal thin-film formation, ensuring homogeneous dispersion of the drug within the lipid matrix. The use of a flask with a volume five times greater than the solution volume (*e.g.*, a 50 mL flask for 10 mL of PC/ERY solution) favoured the formation of a uniform, transparent thin film covering the flask's inner surface. The thin film was produced under controlled conditions of 120 rpm at 45 °C, ensuring gradual solvent evaporation and the formation of a continuous, defect-free thin film, as confirmed under UV light (Fig. S6).

The thin film was hydrated using either PBS (pH 7.4) or water at 37 °C (Table S2). Compared to water, PBS provided lower PDI, likely due to its ionic strength, which reduced ERY's solubility in the hydration medium, promoting its incorporation into liposomes while enhancing liposomal integrity.[37] Moreover, PBS was chosen due to its physiological relevance, mimicking the ionic composition and pH of biological fluids. Hydration was performed at 37 °C to ensure that the lipid bilayer remained in a fluid phase, facilitating the reorganization and self-assembly of liposomes under magnetic stirring. The optimal hydration time, assessed based on reduced turbidity, was 60 hours.

After hydration, the liposomal suspensions were subjected to extrusion through 100 nm, 200 nm and 400 nm polycarbonate membranes at 37 °C. The temperature was chosen to ensure adequate lipid fluidity, for efficient passage through the membranes. The size reduction process required 21 extrusion cycles
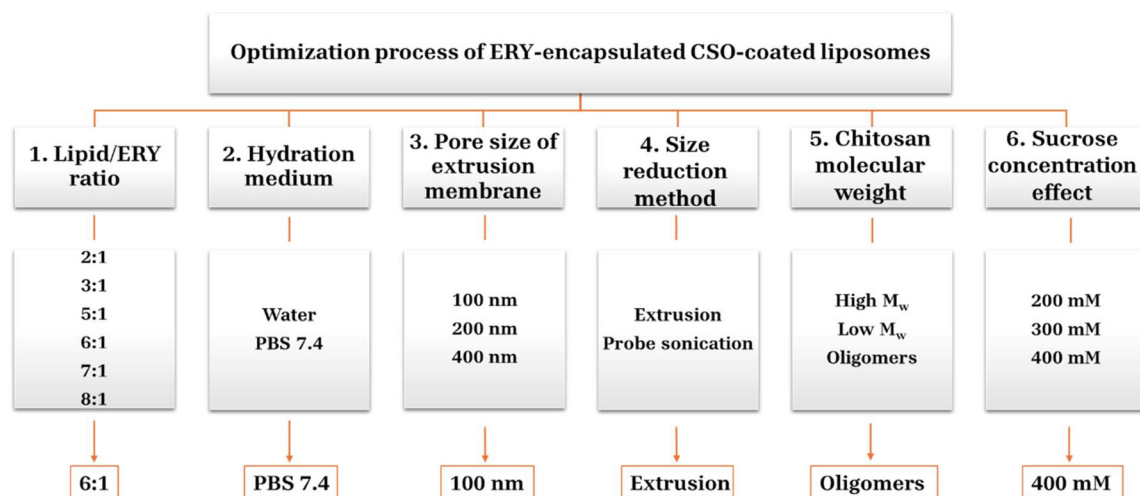
Scheme 1 Brief representation of the optimization process of ECL liposomes.

to reach nanometric size and PDI narrowing. As expected, the size of the liposomes was directly proportional to the diameter of the membrane pores; extrusion through a 100 nm polycarbonate membrane resulted in the formation of the smallest liposomes (Table S3). Liposomes prepared by extrusion exhibited significantly greater size reduction compared to those obtained through sonication. Both bath and probe sonication methods were notably less effective, yielding liposomes with diameters more than twice as large (Tables S4 and S5).

To enhance stability and prevent liposome aggregation, the extruded liposomes were coated with chitosan. Based on the variation of chitosan concentration (Tables S4 and S5) and molecular weight (Table S6) it was determined that the dropwise addition of extruded liposomes into a 0.5% solution of chitosan oligomers (2 kDA) yielded a uniform liposomal coating that effectively prevented aggregation. Higher molecular weight chitosan (302 or 126 kDa) or higher concentrations (1%) resulted in inter-liposomal bridging and subsequent coalescence, most probably a consequence of higher viscosity and insufficient disentanglement of chitosan macromolecules leading to the entanglement of multiple liposomes rather than forming a discrete coating (Fig. S1 and S2).[26,38]

To further improve liposomal stability and enable the conversion into dry powder for prolonged storage or inhalable formulations, the suspensions were stabilized using sucrose as a cryoprotectant.[39] By varying the sucrose concentration from 200 to 400 µM, it was confirmed that an increased sucrose concentration led to the preservation of liposome characteristics postlyophilization and improved rehydration (Table S7 and Fig. S3, S4).[40] Prior to freeze-drying, liposomes underwent dialysis at 0 °C (below the lipid transition temperature), to remove unencapsulated erythromycin while maintaining liposomal integrity.[41] Dialysis was performed in PBS medium containing sucrose, in similar composition with the liposomal suspensions, in order to ensure a proper osmotic balance. Lyophilization successfully preserved liposome morphology, as confirmed by DLS and STEM, which revealed that the rehydrated liposomes maintained their original size distribution and structural integrity (Fig. S3 and S4). A schematic representation of the preparation of ERY liposomes is provided in Fig. 1.

3.2. Physico-chemical investigation

3.2.1. Spectroscopic characterization. The FTIR spectra of ECLs confirmed the presence of all individual components despite some degree of spectral overlap. Comparative analysis of the spectra revealed characteristic vibrational bands corresponding to ERY, PC, and CSO, supporting the successful formulation of the liposomal system (Fig. 2a).

The presence of ERY was evidenced by distinct absorption bands, including the stretching vibration of the carbonyl group in the lactone ring at 1715 cm^{-1} and 1378 cm^{-1}, the
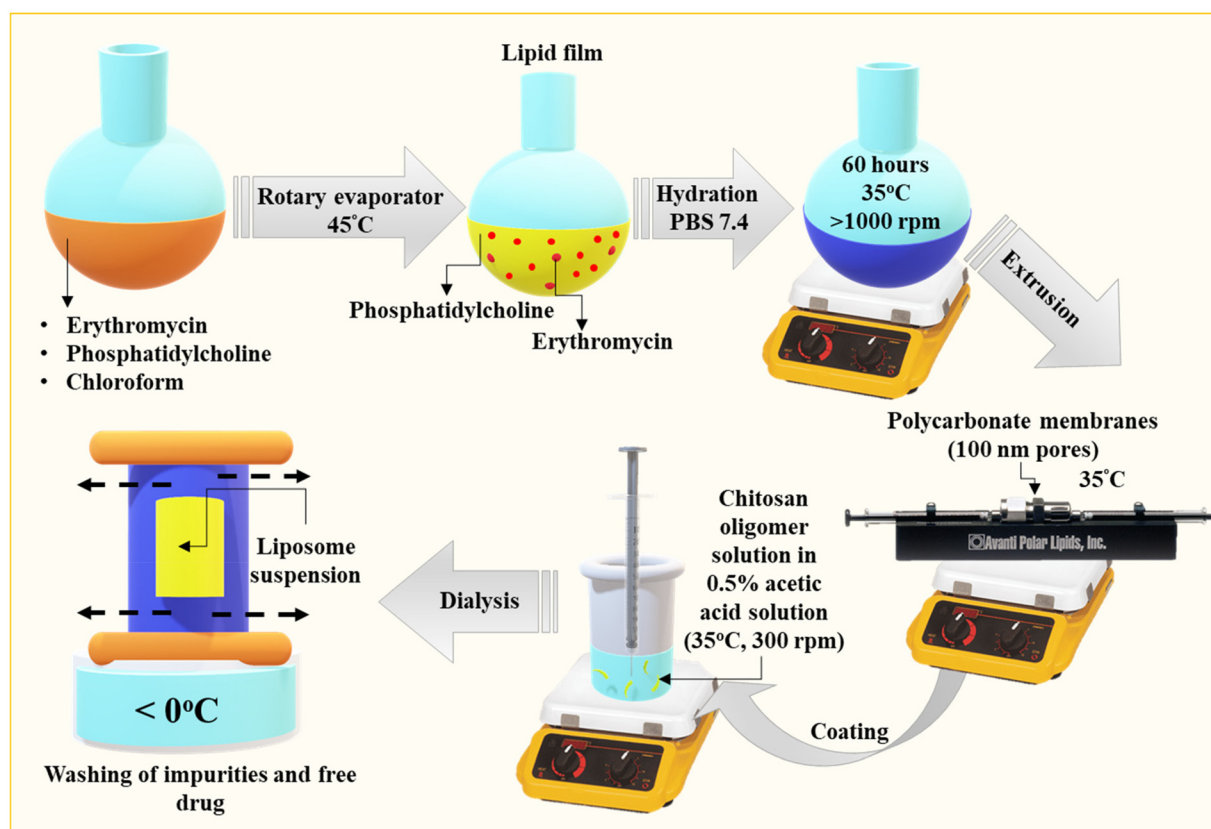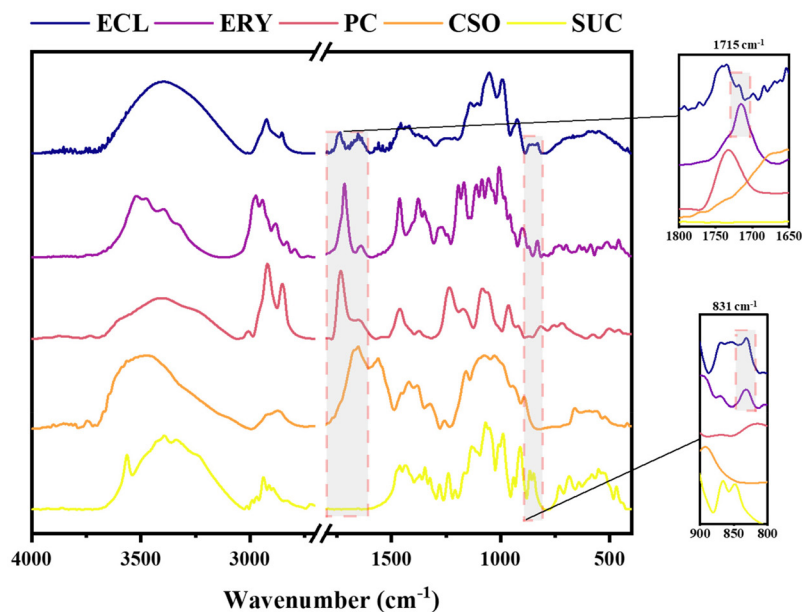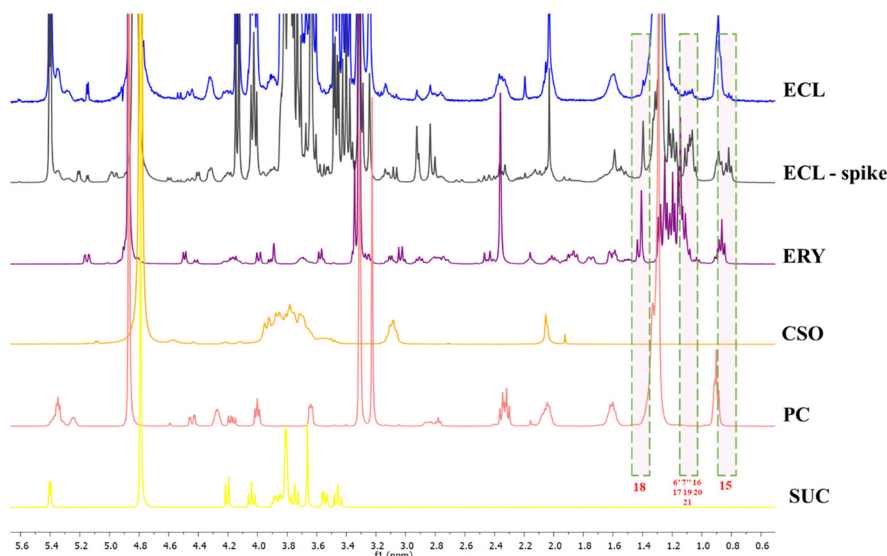

Fig. 1 Schematic representation of CSO-coated ERY liposomes preparation.

Fig. 2 Representative (a) FTIR and (b) ^{1}H-NMR spectra of the studied liposomes and neat components (ECL-spike was prepared by adding ERY in order to better observe its signals).

vibration of the N(CH$_3$)$_2$ group at 1455 cm^{-1}, the C–O stretching vibration at 1080 cm^{-1}, and the N–H bending vibration at 831 cm^{-1}.[42,43]

The spectral features of PC were also clearly distinguished, particularly the C–H stretching vibrations at 2900 cm^{-1} and 2800 cm^{-1}, along with the typical stretching vibrations of the C=O and C–O–P groups at 1720 cm^{-1} and 1022 cm^{-1}, as well as the angular bending of methyl groups of the trimethylammonium units around 1477 cm^{-1}.[44,45]

Furthermore, the characteristic bands of chitosan were present, including the amide II stretching vibration at 1650 cm^{-1}, the amine group absorption at 1560 cm^{-1}, and the broad absorption band starting at the same edge of 3000 cm^{-1}, representative for the hydroxyl and amine groups involved in hydrogen bonding.[29] All these spectral assignments confirmed the successful incorporation of ERY within the liposomal formulation and the presence of chitosan as a stabilizing component.

A closer look reveals slight shifts of the vibration bands of the liposomes' components, in line with physical interactions between them. Thus, the absorption bands belonging to the carbonyl and amine bonds of ERY, shifted to higher wavenumbers

(from 1715 to 1719 cm^{-1} and from 831 to 837 cm^{-1}) in line with their weaknesses due to H-bond formation.[46] Furthermore, the distinctive bands of the carbonyl, phosphate and quaternary groups shifted to lower/higher wavenumbers, also in agreement with their involvement in electrostatic/physical interactions (Fig. S17). The deconvolution of the 3000–3700 cm^{-1} region, consistent with the vibration of hydroxy and amine groups, and the H-bonds between them, displayed the occurrence of 33 bands, pointing for an intricate network of H-bonds between the formulation's components (Fig. S17).

^{1}H-NMR spectroscopy was employed as a complementary method to confirm the presence of individual components within the ECL formulation, with a particular focus on verifying the incorporation of ERY (Fig. 2b). To enhance the detection of ERY signals amidst overlapping spectral regions, a spiking experiment was conducted by adding an additional amount of ERY to the sample. This resulted in an increased intensity of characteristic ERY resonances, notably at 0.8 ppm and 1.4 ppm, which correspond to the protons of methyl groups of the lactone ring. Additionally, distinct signals in the 1.0–1.3 ppm range were assigned to the methyl groups attached to the dimethylamine ($N(CH_3)_2$) moiety, further confirming the presence of ERY within the liposomal system.[47] Additionally, the resonance at ~3.1 ppm characteristic to the H_2 proton of chitosan oligomers was also evident in the ECL spectra, further validating the successful coating of the liposomes.[29] Slight shifting of the signals of protons belonging to ERY were detected, confirming the modification of their chemical environment, most probably due to their implication in H-bonding network.[48] Thus, these NMR findings, in conjunction with FTIR analysis, provide qualitative evidence for the successful encapsulation of ERY within the liposomal formulation and their coating with chitosan oligomers, suggesting the structural integrity and composition of the developed ECL system.

A quantitative assessment of ERY's encapsulation in liposomes was conducted by measuring the encapsulation efficiency (EE%) using UV-VIS spectroscopy on sucrose-free samples, to avoid any potential interference in the absorbance measurements. The EE% was determined to be 62.88 ± 2.19%, which is in the range of previously reported data (from 23% to 87%), with results varying depending on the lipid composition, preparation method, hydration conditions and presence of other ingredients, such as magnetic nanoparticles.[5] It is important to note that in contrast to studies reporting higher EE% for vesicles larger than 200 nm, the liposomes developed in this study exhibit sizes below 100 nm. It is known that smaller liposomes typically display lower encapsulation efficiency due to their limited internal volume.[49] However, they offer advantages such as improved cellular uptake, enhanced distribution, greater stability, favourable biodistribution, and refined tissue penetration.[50,51]

3.2.2. Physical state *via* X-ray diffraction and polarized light microscopy. The physical state of a formulation plays a critical role in determining the bioavailability and stability of the active pharmaceutical ingredients.[52] To evaluate the physical state of its components within the liposomal formulation, X-ray diffraction analysis of the ECL sample was performed and compared with its individual constituents (Fig. 3a).

Plain sucrose exhibited a diffraction pattern specific to its crystalline state, with distinct reflections spanning from 8.5° to 46.3° 2θ.[53] Similarly, pure ERY displayed sharp reflections between 3.7° and 29.6° 2θ, indicative of its crystalline nature, either in hydrated or dehydrated forms.[54] Chitosan oligomers presented a diffraction pattern with two predominant sharp reflections around 10° and 20° 2θ, which are consistent with their semi-crystalline nature, with crystalline domains interspersed within an amorphous matrix.[29,55]

In contrast, the XRD pattern of the ECL formulation revealed a broad halo with a maximum at approximately 20.7°
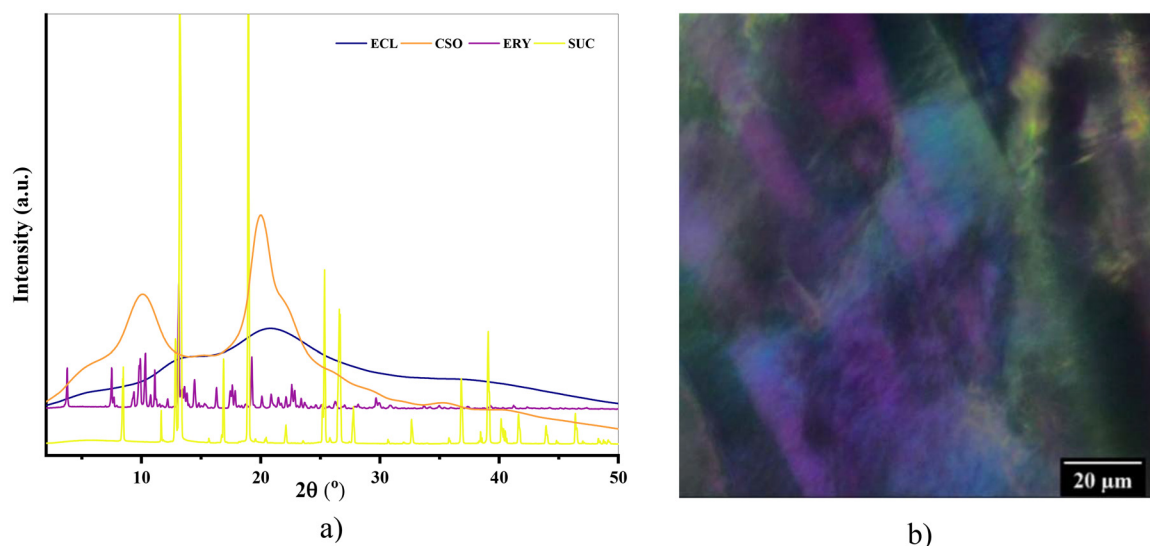

Fig. 3 (a) WXRD diffractograms of ECL and neat components and (b) POM image of ECL.

and a shoulder around 13.1°, resembling the diffractogram of amorphous sucrose.[53] This finding aligns with the high sucrose content in the liposomal composition (~86%, Table 1), which may undergo amorphization upon lyophilization as other researchers reported.[56] The amorphous sucrose likely acts as a cryoprotectant, preventing liposome fusion during the drying process.[57]

The absence of characteristic ERY reflections in the ECL diffractogram suggests that the drug is molecularly dispersed within the lipid bilayer, forming a solid solution and assuming an amorphous state.[58] However, the presence of nanocrystalline domains cannot be entirely ruled out, as they may fall below the detection limit of XRD. To this aim, a complementary analysis was performed using variable temperature POM. At room temperature, POM revealed slightly birefringent domains, although their precise attribution remains uncertain, as PBS salts may also contribute to the observed birefringence (Fig. 3b and Fig. S7). A valuable insight regarding the liposomes' state was gained by POM observations under a heating/cooling cycle. The chitosan-coated liposomes showed no visible changes upon heating up to 200 °C, indicating high thermal stability. In contrast, uncoated liposomes began to melt around 70 °C, the melting point of PC, forming an amorphous film that remained unchanged upon further heating to 200 °C, followed by cooling to room temperature. However, in the following 24 hours, slight birefringent domains appeared within this amorphous film, attributable to the slow crystallization of ERY that had leaked from the liposomes during the PC melting process (Fig. S8). This thermal behaviour highlights, on one hand, the enhanced thermal stability imparted by the chitosan coating, in line with chitosan's known high thermal stability, and on the other hand, supports the XRD findings regarding the amorphous state of ERY within the liposomes.

3.2.3. Morphology through DLS, STEM and AFM. DLS measurements were conducted to evaluate the formation, size distribution, and stability of the ERY loaded liposomes, by measuring the hydrodynamic diameter, polydispersity index (PDI), and zeta potential (ζ-potential) (Fig. 4a–c and Fig. S9–S11). Prior to coating, the liposomes exhibited a size of 95.14 ± 1.64 nm and a ζ-potential of −4.72 ± 0.83 mV. Upon coating with CSO, a slight increase in size to 97.38 ± 0.75 nm was observed, along with a significant shift in ζ-potential to 9.09 ± 1.09 mV. This positive surface charge confirms successful chitosan adsorption on the surface of liposomes, expected to enhance colloidal stability by preventing aggregation. Compared to liposomes coated with high molecular weight chitosan (Tables S1 and S3), those coated with CSO displayed a significantly lower ζ-potential, but they also exhibited lower size and PDI (<0.1) pointing for their improved homogeneity, which is critical for ensuring reproducibility in drug delivery applications.

Interestingly, the ERY-loaded liposomes (EL, ECL) displayed a statistically significant reduction in size compared to plain liposomes (CL), suggesting a more compact morphology (Fig. 4a), attributed to the increased surface curvature induced by intermolecular interactions between lipid and ERY.[59,60] The lower PDI values of loaded EL and ECL liposomes, relative to plain CL liposomes, further support this structural rearrangement (Fig. 4b).

Coating with CSO induced the increase of ζ-potential in both plain and ERY-loaded liposomes, confirming CSO as the primary contributor to the positive surface charge (Fig. 4c). Notably, the negative ζ-potential of uncoated ERY liposomes suggests that interactions between the positively charged PC headgroups and the electron-rich functional groups of ERY (hydroxyl, carbonyl, and amine) lead to charge redistribution, exposing negative charge at the surface. It is expected as upon CSO coating, the positively charged protonated amine groups of chitosan to electrostatically interact with the negatively charged sites of PC, forming a stable coating and further enhancing colloidal stability.[61,62]

STEM images confirmed the presence of spherical vesicles which are characteristic of liposomes (Fig. 4d and e). The measured average diameter of 97.72 ± 21.09 nm aligns well with the DLS results, reinforcing the hypothesis of a compact structural arrangement facilitated by intermolecular interactions between ERY and PC. Additionally, salt crystallization from the suspension medium was occasionally observed interspersed among the lipid aggregates. When STEM samples were prepared directly from the undiluted ECL suspension, the vesicles appeared closely packed, yet well-defined, with distinct spherical morphology and uniform size distribution (Fig. 4d). In contrast, dilution of the suspension before sample preparation led to rarer vesicles, revealing a densely packed core, attributable to the strong ERY-PC molecular interactions, surrounded by a looser, rough outer shell, corresponding to the CSO coating. A similar outer shell was observed in the CL liposomes but was absent in the EL samples, supporting its identification as the CSO coating. Additionally, the uncoated EL liposomes exhibited clear signs of coalescence and film formation, further confirming the stabilizing effect of the CSO coating (Fig. S12). Notably, no lamellar structures were observed, suggesting either that the liposomes are unilamellar or that the CSO coating, due to its different electron density compared to the lipid bilayer, may obscure the visualization of lipid layers under STEM, or a very close packing via H-bonding network between the ERY and PC. AFM and SEM analysis of the ECL lyophilised sample confirmed the presence of intact, rounded vesicles embedded within an amorphous sucrose matrix (Fig. 4f and g).

The agreement between STEM and DLS measurements emphasizes the stabilizing effect of the CSO coating, which limits the aggregation and promotes a compact, uniform morphology, which are key attributes for potential biomedical applications (Fig. S13).

3.2.4. Storage stability. The stability of ERY-loaded liposomes coated with CSO was evaluated over a two-month period by monitoring changes in particle size and PDI at three different temperatures: 5 °C, 25 °C, and 50 °C. As shown in Fig. 5a, b and Fig. S14 liposome diameter increased progressively over time, with a statistically significant rate, nearly tripling for those stored at 50 °C. Interestingly, 25 °C appeared to
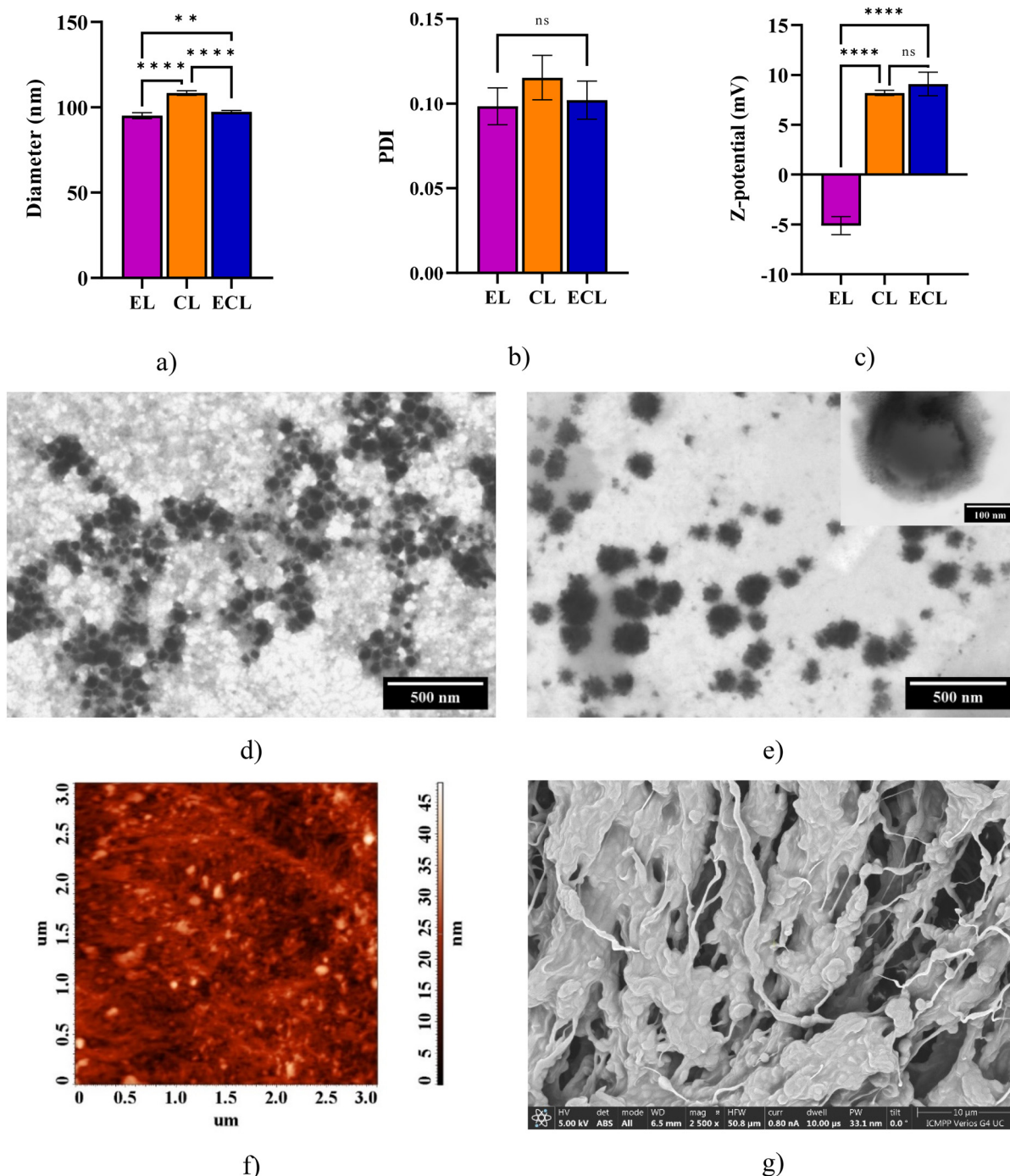
Fig. 4 Comparative representation of (a) size, (b) PDI and (c) ζ-potential of ECL liposomes compared to EL and CL references; STEM images of ECL when prepared by casting from (d) as obtained suspension and (e) diluted 10 times (scale bar: 500 nm, in inset: 100 nm); (f) AFM (scale bar: 3 µm) and (g) SEM image of freeze-dried and redispersed liposomes (scale bar: 10 µm) (ns: nonsignificant statistic; **$p < 0.01$,****$p < 0.0001$).

be an optimal temperature for storage of the liposomal formulations, with the lowest size increase over 6 weeks. It can be envisaged that a diminished or accelerated Brownian movement of the liposomes at 5 and 50 °C, respectively, is more conducive to effective collisions, leading to flocculation, discernible to the naked eye after 8 weeks (Fig. 5c and Fig. S15). However, despite these changes, the liposomal formulation remained well within the nanometric range, in contrast to other reported formulations where ERY liposomes initially exceeded 200 nm in diameter.[5] These findings suggest that the optimized formulation exhibits relatively good stability even in the absence of a lipoprotectant, allowing for suspension storage for at least 6 weeks while preserving key physicochemical characteristics.
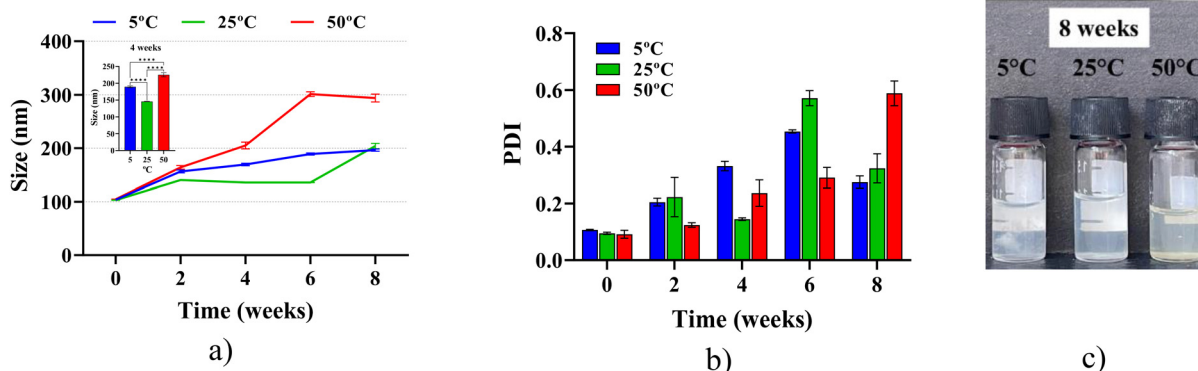
Fig. 5 (a) Size, (b) polydispersity index, and (c) imaging data of the ECL liposomal formulation stored at various temperatures over an 8-week period; inset in (a) graphical representation of liposome size after 4 weeks of storage; ****p < 0.0001.

3.3. *In vitro* release of ERY

The release of ERY in pure form through dialysis membranes occurred rapidly (less than 4 hours), while drug release from the liposomes occurred gradually over the first 10 hours, with a slightly faster release observed in the presence of enzymes, 77% *vs*. 70%, and a subtle burst effect in the first 2 hours (Fig. 6). These results support the idea of a sustained drug release model, where the gradual biodegradation of chitosan serves as a rate-controlling mechanism, delaying the release process and acting as a trigger for drug diffusion from the formulation. Compared to other previously reported ERY-loaded liposomes, the release profile established in this study appeared to be more sustained, highlighting the protective and controlled-release effect of the CSO coating.[5]

The release kinetics of ERY from ECL and neat ERY were investigated by fitting the release profiles to five commonly used kinetic models, while the best-fitting model was evaluated based on the correlation coefficient (R^2) (Table 2). The

Hixson–Crowell model (R^2 = 0.99) suggests a release mechanism influenced by erosion of the liposomal matrix, which may be especially relevant in the presence of enzymes. The Higuchi model (R^2 = 0.98) also fit well, indicating a diffusion-controlled release mechanism. Low R^2 values obtained by fitting the Korsmayer–Peppas model may not reflect a meaningful physical mechanism and suggest that this model is not suitable here. Thus, the release of ERY from liposomes appeared to follow a combination of diffusion (Higuchi) and matrix erosion (Hixson–Crowell), with contribution from zero-order kinetics, indicating sustained and controlled release behaviour, especially when enzymes are present to degrade the chitosan coating. In the case of neat ERY, R^2 values are significantly lower across all models (R^2 till 0.89), indicating poor fitting compared to liposomal formulations. The best fit was for the Higuchi model, suggesting that diffusion is the primary mechanism governing release. Weak fits of the other models suggests that free ERY release is less controlled and likely more erratic and abrupt.
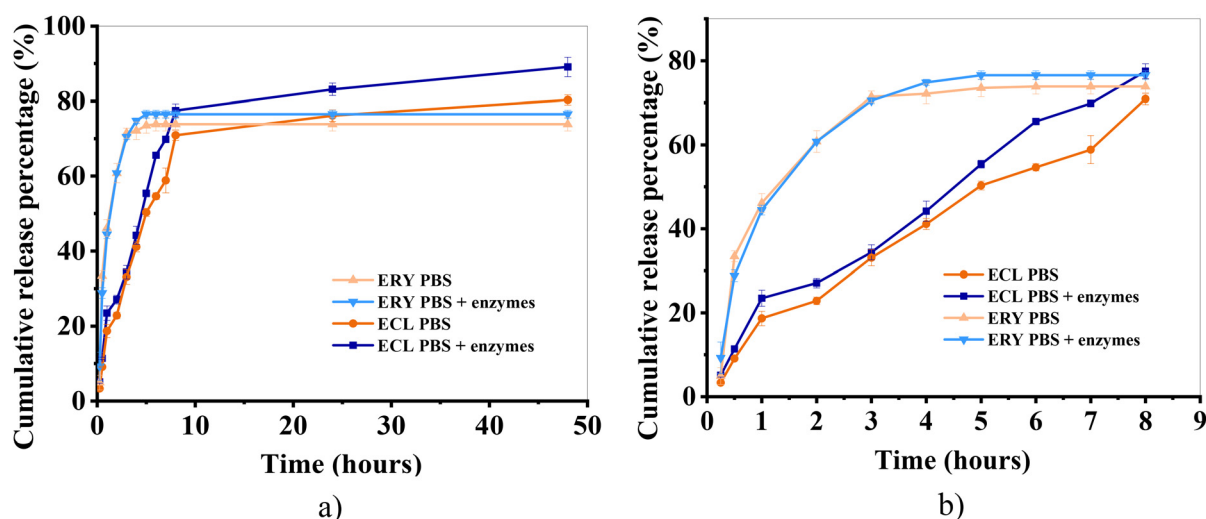

Fig. 6 Release kinetics of ERY from ECL compared to blank ERY, in both PBS and PBS with lysozyme and lipase over (a) 48 and (b) 8 hours.

Table 2 Parameters of the different model fitting on experimental release data

Code	Zero order		First order		Higuchi model		Hixson–Crowell		Korsmeyer–Peppas		
	R^2	K_0	R^2	K_t	R^2	K_H	R^2	κ	R^2	k	n_r
ECL PBS	0.98	0.13	0.98	−0.00230	0.98	3.52	0.99	−0.003	0.12	0.03	0.36
ECL PBS + enzymes	0.98	0.15	0.98	−0.00299	0.98	3.90	0.99	−0.004	0.57	0.03	0.77
ERY PBS	0.78	0.26	0.89	−0.00530	0.89	4.65	0.86	−0.006	0.19	0.14	−0.84

3.4. Biological activity

3.4.1. Mucoadhesivity. Chitosan is widely regarded as the gold standard for mucoadhesive properties of biomaterials, owing to its structure rich in hydroxyl and amine/protonated amine functional groups, which are capable of forming strong electrostatic and hydrogen bonds with mucosal membranes and epithelial tissues.[63] In the context of liposomes, this property is expected to be even more pronounced due to their high surface-to-volume ratio.

To assess mucoadhesivity, we evaluated changes in transparency upon contact with mucin (Fig. 7). Initially, plain liposomal suspensions, both chitosan-coated (CL, ECL) and uncoated (EL), exhibited high transparency, with light transmittance ranging from 39.09% to 64.81%. As expected, chitosan-coated liposomes were less transparent, consistent with the higher refractive index of chitosan compared to phosphatidylcholine, and the increased surface roughness of the coated liposomes, both of which enhance light scattering and contribute to greater turbidity.[64,65] In contrast, mucin alone formed highly opaque solutions, with transmittance around
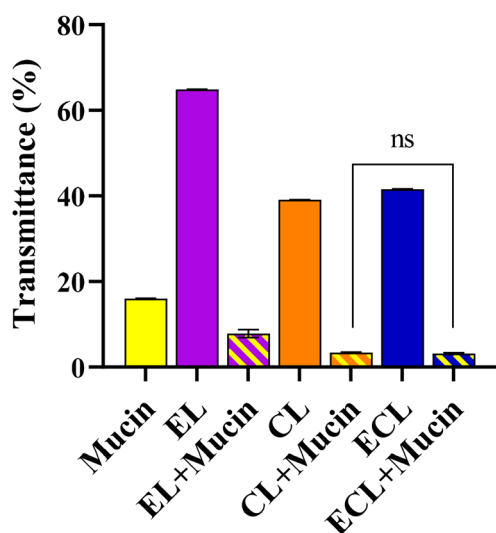

Fig. 7 Transmittance of the mucin and liposomal suspensions (from statistical analysis, all samples have a $p < 0.0001$ when compared to other samples/same sample after incubation with mucin, except for those shown on the graphic).

18%, as previously reported.[66,67] This opacity is attributed to the self-association and aggregation of mucin macromolecules, leading to gel-like architectures. Based on this premise, it would be expected that mixing liposomes with mucin would result in intermediate transparency. Contrary to this expectation, upon mixing the two, the transparency dropped significantly, with chitosan-coated liposomal formulations reaching transmittance as low as 3.09%. Notably, uncoated liposomes maintained higher transparency in the mucin mixture compared to coated samples (Fig. 7). This further confirms the contribution of chitosan to the enhanced turbidity.

The sharp increase in mucin turbidity upon mixing with liposomes is attributed to the promotion of mucin aggregation, likely mediated by nanometric liposomes through physical interactions such as hydrogen bonding.[66] In the case of EL liposomes, the turbidity increase can be explained by the interaction of zwitterionic PC with mucin proteins via interfacial, non-classical interactions.[68] For chitosan-coated liposomes, the pronounced turbidity is due to the strong hydrogen bonding capacity of chitosan with mucin macromolecules.[35,67]

These results indicate excellent mucoadhesive properties of the chitosan-coated liposomes, suggesting an extended residence time on mucosal tissues and, consequently, enhanced adsorption and prolonged release of erythromycin. This finding is particularly noteworthy, as, based on current literature, there appear to be no prior reports addressing the mucoadhesive properties of ERY formulations incorporating chitosan.[69,70]

3.4.2. Antioxidant activity. Antioxidant activity was evaluated using the DPPH radical scavenging assay (Fig. 8). To assess the contribution of individual liposomal components, each one was first tested independently. As expected, CSO exhibited strong antioxidant activity, with an 80% DPPH radical scavenging rate, consistent with previous findings.[71] By comparison, free ERY showed modest antioxidant activity (~20%), which aligns with its molecular structure rich in hydroxyl groups capable of donating electrons to neutralize free radicals.[72] PC demonstrated slightly higher scavenging activity (~30%), in agreement with literature values, likely due to the presence of the choline headgroup containing amine and hydroxyl functionalities that can participate in redox reactions.[73,74]

The tricomponent ECL formulation exhibited a concentration-dependent antioxidant response, with the undiluted
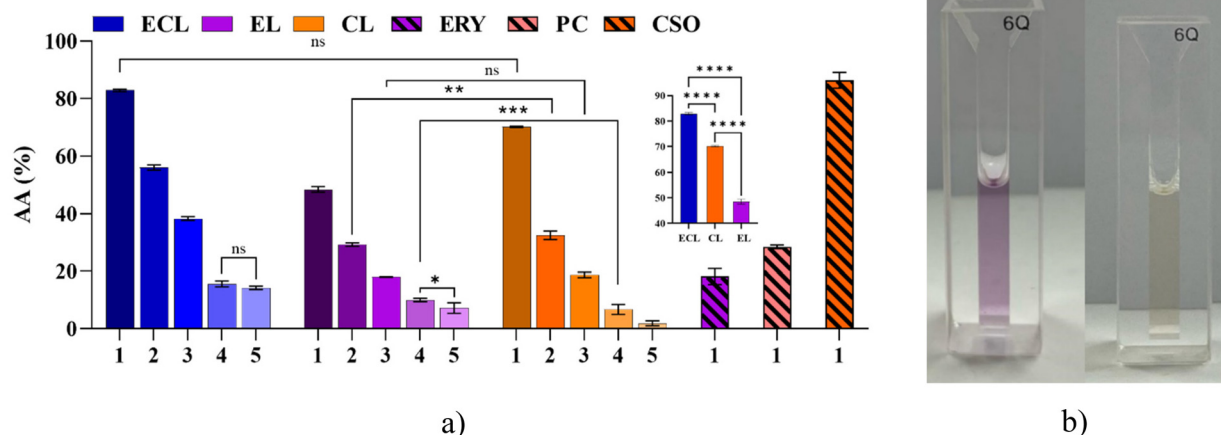
Fig. 8 (a) Graphical representation of the antioxidant activity of tested samples against neat ERY, PC and CSO; (b) image of ECL sample before and after incubation with DPPH (*$p < 0.05$; **$p < 0.01$; ***$p < 0.001$; ****$p < 0.0001$) (on OX axe, the increasing numbers signify the dilution increase: 1 = 1/0; 2 = 1/1; 3 = 1/3; 4 = 1/7; 5 = 1/15, v/v).

suspension reaching approximately 80% radical scavenging activity. Upon serial dilution (up to 1 : 15), the activity progressively decreased, reaching a minimum of 14.27%. Notably, the decline in antioxidant activity was not strictly proportional to dilution, attributable to the occurrence of intermolecular interactions, such as hydrogen bonding and electrostatic forces, between functional groups involved in radical scavenging. The strength of such forces is expected to weaken along with dilution, making the functional groups available for radical binding. This is further supported by the observation that the antioxidant activity of the ECL formulation was lower than the cumulative activity of its individual components, indicating possible structural constraints or altered accessibility of active sites in the vesicular system.

Comparative analysis among the formulations showed that chitosan plays a dominant role in antioxidant performance. The chitosan-coated liposomes without ERY (CL) displayed statistically higher scavenging activity than uncoated erythromycin-loaded liposomes (EL), emphasizing chitosan's strong contribution. However, both bicomponent CL and EL formulations showed statistically significant reduced activity compared to the tricomponent ECL sample, highlighting the cumulative/synergistic effect of incorporating all three components: CSO, PC, and ERY. It is worth emphasizing that, although the combination of ERY with antioxidant agents to enhance multifunctionality has been explored in chitosan-based hydrogels, the intrinsic antioxidant-promoting role of chitosan itself has not been previously considered, this study reporting it for the first time.[70]

Overall, these findings confirm that ECL liposomes possess significant antioxidant capacity. This feature may be particularly advantageous in therapeutic applications, as it can help mitigate oxidative stress at the site of administration, reduce inflammation, combat infection, and protect host cells, especially in treatments targeting sensitive or inflamed tissues.[75]

3.4.3. Antibacterial activity. The antibacterial activity was investigated following two methods, disk diffusion assay and time-kill kinetics screening, on two representative strains: Gram positive *E. faecalis* and Gram negative *K. pneumoniae*.

In the disk diffusion assay, ECL liposomes presented the same activity as neat ERY against both tested bacterial strains, being more efficient against *E. faecalis* (around 22 mm of inhibition zone) than *K. pneumoniae* (around 15 mm of inhibition zone) (Fig. 9a and b). This was attributed to ERY's well-known superior efficacy over Gram positive species. Sample CL exhibited no detectable antibacterial activity (Table S8), likely due to the low concentration of chitosan.[76,77]

To gain a deeper insight into the antibacterial efficacy of the studied formulations, time-kill kinetics assays were performed using the same bacterial strains as in the disk diffusion assay. Unlike the latter, this dynamic method revealed clear, strain-dependent differences in bacterial susceptibility.

For the Gram-positive strain *E. faecalis* (Fig. 9c and e), free ERY demonstrated a gradual reduction of bacterial viability to 42% after 6 hours of incubation. In contrast, ERY-loaded liposomes exhibited a markedly faster antibacterial response, reducing viability to 2% within 4 hours and further to 0.6% by the 6-hour mark.

In the case of the Gram-negative strain *K. pneumoniae*, both free ERY and ECL demonstrated similar antibacterial activity over the first 6 hours, reducing bacterial viability to approximately 45%, with no notable enhancement from the liposomal formulation (Fig. 9d and f).

The superior performance of ECL against *E. faecalis* suggests that the chitosan coated liposomes may facilitate direct interaction with, or internalization through, the Gram-positive bacterial wall, which lacks an outer membrane, making the surface accessible for electrostatic interactions with the cationic chitosan. This structural feature of Gram-positive bacteria likely allows more efficient fusion or translo-
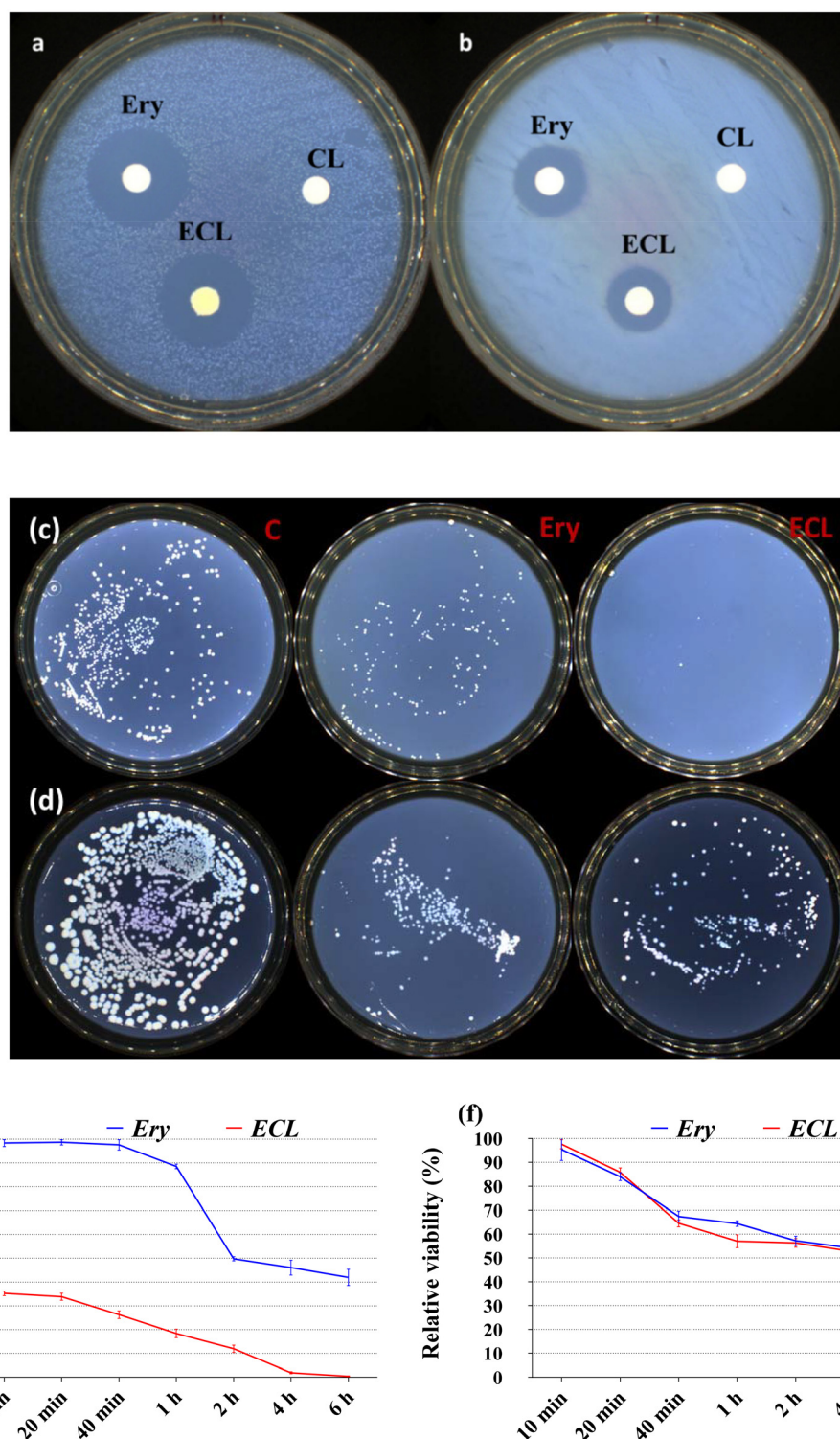
Fig. 9   Inhibition zone determined by disk diffusion assay against: (a) *E. faecalis*, and (b) *K. pneumoniae* and microbial growth inhibition determined by time kill kinetics against (c), (e) *E. faecalis* and (d), (f) *K. pneumoniae* expressed as percent of viable bacterial colonies *vs.* incubation time over 6 hours (C: control).

cation of the chitosan coated liposomes, enabling enhanced intracellular delivery of ERY and thus achieving higher localized concentrations of the antibiotic. This mechanism appears to convert erythromycin's traditionally bacteriostatic mode of action into a bactericidal effect, through sustained and targeted drug release.[78,79]
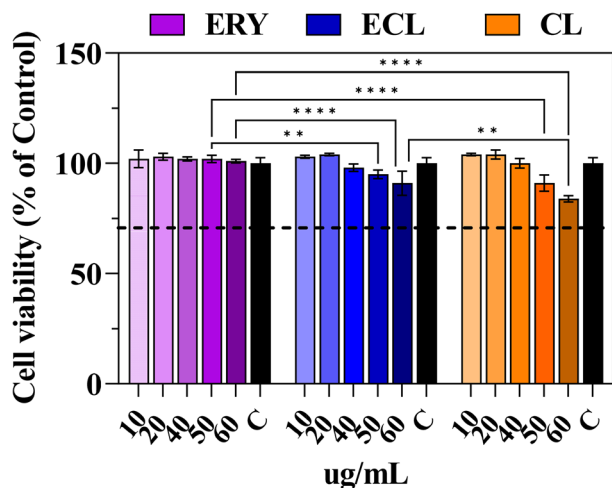
Fig. 10 Cell viability of normal human gingival fibroblasts after 24 h exposure to liposomal formulation, compared to untreated cells (C) (**p < 0.01, ****p < 0.0001) (the dashed line indicates the 70% cell viability threshold).

Conversely, the cell wall of Gram-negative bacteria such as *K. pneumoniae*, which has an outer membrane rich in lipopolysaccharides, acts as a barrier to both liposomes and chitosan, while also limiting the uptake of hydrophobic molecules such as ERY, as well as large carriers, including liposomes.[80] This structural barrier likely explains the similar activity observed for both free and encapsulated ERY.

However, the stronger effect against Gram-positive bacteria compared to Gram-negative bacteria is not surprising, as this trend is commonly reported.[81] When comparing our results to other studies on various ERY formulations tested against Gram-positive cocci, a similar improvement in ERY activity was observed, when encapsulated in liposomes, chitosan nanoparticles, or other chitosan biomaterials (Table S9).[69,82–92] This supports the idea that both lipids and chitosan play a role in enhancing the antibiotic's efficiency.

Most importantly, the accelerated and near-complete eradication of *E. faecalis* by ECL is clinically relevant, as it may help in infection prophylaxis, inhibit biofilm formation, and reduce the risk of resistance development, as reported in previous studies.[93,94] Additionally, faster bacterial clearance may contribute to shorter treatment durations, offering a significant advantage in therapeutic contexts.[95]

3.4.4. Cytocompatibility. For *in vivo* applications, the lack of cytotoxicity of liposomes is essential. In order to evaluate their potential for real-world applications, the cytotoxicity of the studied liposomes was assessed using normal human gingival fibroblasts (NHGF) as a model for normal human cells (Fig. 10). Throughout the tested concentration range (10–60 μg mL^{-1}) and a 24-hour exposure time, neither the liposomal formulation nor ERY exhibited cytotoxic effects, thereby fulfilling the biocompatibility criteria established by ISO 10993-5:2009 for biomedical devices.[36]

Free ERY maintained 100% cell viability, consistent with previous studies reporting no cytotoxicity at doses below 200 μg mL^{-1} when tested on BALB/C 3T3 fibroblasts.[96,97] Notably, CL liposomes demonstrated a dose-dependent effect, with a slight decrease in cell viability to 85% at the highest tested concentration. This finding is particularly relevant given that phosphatidylcholine, a major component of cell membranes, is generally considered non-cytotoxic when used at concentrations below 10%, making it a safe and widely accepted excipient in pharmaceutical formulations.[98,99] Chitosan oligomers are also regarded as cytocompatibile, even though some studies suggest that their cytotoxic effect depends on the degree of deacetylation and testing method. However, while initial cell viability may have been slightly reduced within the first 24 hours, overall values remained within the biocompatibility limits defined for biomedical applications, aligning with our findings.[100,101] This behaviour is attributed to the presence of protonated amine groups, which interact with cellular components. Interestingly, the ERY-loaded liposomes exhibited significantly higher cell viability compared to CL liposomes, suggesting that the presence of ERY may contribute to the overall cytocompatibility of the liposomal formulation. This is a controversial finding, considering the fact that other studies have reported either no impact or slight reduction of cell compatibility when loading ERY into hydrogels,[90] microcapsules,[102] or nanoparticles.[103] Nevertheless, similar results to those presented in the current study were also reported for liposomes loaded with ERY derivatives[104] and ERY loaded into chitosan nanofibers,[86] suggesting that the small differences observed may be due to variations in experimental conditions, such as the amount of tested material, the nature of the carrying material or the type of cells used.

4. Conclusions

This work highlights the successful development and optimization of erythromycin-loaded liposomes coated with chitosan oligomers, showcasing a formulation with superior functional and structural properties. Through systematic parameter tuning, a balance was achieved between high encapsulation efficiency, nanoscale uniformity, and a multifunctional profile encompassing enhanced mucoadhesion, sustained antibacterial activity, and strong antioxidant effects. Compared to reported erythromycin formulations, the current optimized liposomes offer several advantages: (i) efficient drug encapsulation into nanometric liposomes with excellent size homogeneity leading to a controlled release governed by diffusion and matrix erosion; (ii) superior antibacterial efficacy, including rapid initial action against Gram-positive strains; (iii) high mucoadhesive properties, supporting targeted delivery to mucosal sites; (iv) robust antioxidant activity, aiding in the reduction of oxidative stress; (v) excellent cytocompatibility, supporting their use *in vivo*; and (vi) good stability which favours the preservation of liposomal properties during freeze-drying and storage at room temperature conditions.

Together, these findings suggest that the developed ERY-liposomes are a viable and versatile platform for therapeutic delivery, with potential to be translated into clinical applications aimed at treating infectious diseases, where bacterial resistance and oxidative stress coexist, particularly at mucosal sites such as the buccal, nasal, ocular, pulmonary, gastrointestinal, vaginal, and rectal mucosae. Although the optimization of both the formulation and preparation process supports the potential for large-scale production, certain limitations remain, particularly the need to assess ERY stability within liposomes under various storage conditions and *in vivo* environments. These aspects must be thoroughly investigated before advancing toward practical, real-world applications.

Author contributions

VMP: investigation, software, writing original draft, methodology, data curation; AMC: investigation, software; IR: investigation, formal analysis, writing original draft; NS: investigation, formal analysis, writing original draft; LM: supervision, formal analysis, writing original draft, writing – review & editing, project administration, conceptualization.

Conflicts of interest

There are no conflicts to declare.

Data availability

The raw/processed data required to reproduce these findings are available at request.

Supplementary information is available. Optimization of ERY liposomes preparation; STEM images of the tested liposomes; POM images of freeze-dried liposomes; DLS curves; FTIR deconvolution; Morphological characteristics and antibacterial activity of ERY formulations reported in literature. See DOI: https://doi.org/10.1039/d5bm00629e.

Acknowledgements

References

1 M. Sun, Z. Xue, J. Li and L. Du, Efficacy and Safety of Erythromycin in the Treatment of Mycoplasma Pneumonia in Children: A Systematic Review and Meta-Analysis, *Indian J. Pharm. Educ. Res.*, 2024, **58**, 1007–1014, DOI: 10.5530/ijper.58.4.113.

2 M. Szczupak, M. Jankowska, B. Jankowski, J. Wierzchowska, J. Kobak, P. Szczupak, J. Kosydar-Bochenek and S. Krupa-Nurcek, Prokinetic effect of erythromycin in the management of gastroparesis in critically ill patients—our experience and literature review, *Front. Med.*, 2024, **11**, 1440992, DOI: 10.3389/fmed.2024.1440992.

3 T. Adamantidi, E. Panoutsopoulou, E. Stavrakoudi, P. Tzevelekou and N. C. Kokkinos, Industrial Catalytic Production Process of Erythromycin, *Processes*, 2024, **12**, 1533, DOI: 10.3390/pr12071533.

4 P. Thevin, C. Curti, A. Benech, C. Jean, E. Lamy, C. Castera Ducros, N. Primas, P. Bertault-Peres and P. Vanelle, Low-dose erythromycin in pediatrics: Formulation and stability of 20 mg hard gelatin capsules, *PLoS One*, 2023, **18**, e0282164, DOI: 10.1371/journal.pone.0282164.

5 V.-M. Platon, B. Dragoi and L. Marin, Erythromycin Formulations—A Journey to Advanced Drug Delivery, *Pharmaceutics*, 2022, **14**, 2180, DOI: 10.3390/pharmaceutics14102180.

6 C.-P. C. Koutsogiannidis and E. O. Johnson, Pharmacological Neuroprotection in Cardiac Surgery: Effectiveness of Pharmacologic-Preconditioning with Erythromycin, *Curr. Vasc. Pharmacol.*, 2018, **16**, 329–335, DOI: 10.2174/1570161115666171010120953.

7 J. Pollock and J. D. Chalmers, The immunomodulatory effects of macrolide antibiotics in respiratory disease, *Pulm. Pharmacol. Ther.*, 2021, **71**, 102095, DOI: 10.1016/j.pupt.2021.102095.

8 A. Ashraf, G. Liu, B. Yousaf, M. Arif, R. Ahmed, S. Irshad, A. I. Cheema, A. Rashid and H. Gulzaman, Recent trends in advanced oxidation process-based degradation of erythromycin: Pollution status, eco-toxicity and degradation mechanism in aquatic ecosystems, *Sci. Total Environ.*, 2021, **772**, 145389, DOI: 10.1016/j.scitotenv.2021.145389.

9 M. Mohsin, I. A. Bhatti, M. Iqbal, S. Naz, A. Ashar, J. Nisar, F. F. Al-Fawzan and S. A. Alissa, Oxidative degradation of erythromycin using calcium carbonate under UV and solar light irradiation: Condition optimized by response surface methodology, *J. Water Process Eng.*, 2021, **44**, 102433, DOI: 10.1016/j.jwpe.2021.102433.

10 M. H. Abdallah, H. A. Elghamry, N. E. Khalifa, W. M. A. Khojali, E.-S. Khafagy, S. Shawky, H. E.-S. El-Horany and S. El-Housiny, Development and Optimization of Erythromycin Loaded Transethosomes Cinnamon Oil Based Emulgel for Antimicrobial Efficiency, *Gels*, 2023, **9**, 137, DOI: 10.3390/gels9020137.

11 N. Mandras, A. Luganini, M. Argenziano, J. Roana, G. Giribaldi, V. Tullio, L. Cavallo, M. Prato, R. Cavalli, A. M. Cuffini, V. Allizond and G. Banche, Design, Characterization, and Biological Activities of Erythromycin-Loaded Nanodroplets to Counteract Infected Chronic Wounds Due to Streptococcus pyogenes, *Int. J. Mol. Sci.*, 2023, **24**, 1865, DOI: 10.3390/ijms24031865.

12 G. Bozzuto and A. Molinari, Liposomes as nanomedical devices, *Int. J. Nanomed.*, 2015, 975, DOI: 10.2147/IJN.S68861.

13 S. Chowdhury, S. Ghosh, M. A. Aleem, S. Parveen, M. A. Islam, M. M. Rashid, Z. Akhtar and F. Chowdhury, Antibiotic Usage and Resistance in Food Animal Production: What Have We Learned from Bangladesh?, *Antibiotics*, 2021, **10**, 1032, DOI: **10.3390/antibiotics10091032**.

14 U. Bulbake, S. Doppalapudi, N. Kommineni and W. Khan, Liposomal Formulations in Clinical Use: An Updated Review, *Pharmaceutics*, 2017, **9**, 12, DOI: **10.3390/pharmaceutics9020012**.

15 P. Liu, G. Chen and J. Zhang, A Review of Liposomes as a Drug Delivery System: Current Status of Approved Products, Regulatory Environments, and Future Perspectives, *Molecules*, 2022, **27**, 1372, DOI: **10.3390/molecules27041372**.

16 N. Mamidi, F. Franco De Silva and A. Orash Mahmoudsalehi, Advanced disease therapeutics using engineered living drug delivery systems, *Nanoscale*, 2025, **17**, 7673–7696, DOI: **10.1039/D4NR05298F**.

17 R. Eugster and P. Luciani, Liposomes: Bridging the gap from lab to pharmaceuticals, *Curr. Opin. Colloid Interface Sci.*, 2025, **75**, 101875, DOI: **10.1016/j.cocis.2024.101875**.

18 H. Hameed, M. A. Khan, A. C. Paiva-Santos, S. Faheem, A. Khalid, M. S. Majid, A. Adnan and F. Rana, Liposomes like advanced drug carriers: from fundamentals to pharmaceutical applications, *J. Microencapsulation*, 2024, **41**, 456–478, DOI: **10.1080/02652048.2024.2376116**.

19 I. Singh, S. Kumar, S. Singh and M. Y. Wani, Overcoming resistance: Chitosan-modified liposomes as targeted drug carriers in the fight against multidrug resistant bacteria-a review, *Int. J. Biol. Macromol.*, 2024, **278**, 135022, DOI: **10.1016/j.ijbiomac.2024.135022**.

20 D. Guimarães, A. Cavaco-Paulo and E. Nogueira, Design of liposomes as drug delivery system for therapeutic applications, *Int. J. Pharm.*, 2021, **601**, 120571, DOI: **10.1016/j.ijpharm.2021.120571**.

21 J.-P. Montenez, F. Van Bambeke, J. Piret, R. Brasseur, P. M. Tulkens and M.-P. Mingeot-Leclercq, Interactions of Macrolide Antibiotics (Erythromycin A, Roxithromycin, Erythromycylamine [Dirithromycin], and Azithromycin) with Phospholipids: Computer-Aided Conformational Analysis and Studies on Acellular and Cell Culture Models, *Toxicol. Appl. Pharmacol.*, 1999, **156**, 129–140, DOI: **10.1006/taap.1999.8632**.

22 F. Zhou, T. Xu, Y. Zhao, H. Song, L. Zhang, X. Wu and B. Lu, Chitosan-coated liposomes as delivery systems for improving the stability and oral bioavailability of acteoside, *Food Hydrocolloids*, 2018, **83**, 17–24, DOI: **10.1016/j.foodhyd.2018.04.040**.

23 P. Wang, S. Zhu, Q. Zhu, X. Yang, C. Wu, K. Liang, Z. He, W. Min, X. Liu, W. Li and F. Wu, Effect of chitosan coating on the characterization and stability of the CPH liposomes, *J. Food Eng.*, 2025, **388**, 112363, DOI: **10.1016/j.jfoodeng.2024.112363**.

24 P. Wydro, B. Krajewska and K. Hąc-Wydro, Chitosan as a Lipid Binder: A Langmuir Monolayer Study of Chitosan−Lipid Interactions, *Biomacromolecules*, 2007, **8**, 2611–2617, DOI: **10.1021/bm700453x**.

25 J. Filipovic-Grcic, N. Škalko-Basnet and I. Jalsienjak, Mucoadhesive chitosan-coated liposomes: characteristics and stability, *J. Microencapsulation*, 2001, **18**, 3–12, DOI: **10.1080/026520401750038557**.

26 A. A. Yaroslavov, A. A. Efimova, E. A. Krasnikov, K. S. Trosheva, A. S. Popov, N. S. Melik-Nubarov and G. G. Krivtsov, Chitosan-based multi-liposomal complexes: Synthesis, biodegradability and cytotoxicity, *Int. J. Biol. Macromol.*, 2021, **177**, 455–462, DOI: **10.1016/j.ijbiomac.2021.02.169**.

27 W. L. Stone, S. Mukherjee, M. Smith and S. K. Das, Therapeutic Uses of Antioxidant Liposomes, in *Liposome Methods and Protocols*, Humana Press, New Jersey, 2002, pp. 145–162. DOI: **10.1385/1-59259-175-2:145**.

28 D. Ailincai, I. Rosca, L. Ursu and A. Dascalu, Chitosan oligomers – Synthesis, characterization and properties, *Cellul. Chem. Technol.*, 2022, **56**, 767–776, DOI: **10.35812/CelluloseChemTechnol.2022.56.68**.

29 D. Ailincai, I. Rosca, S. Morariu, L. Mititelu-Tartau and L. Marin, Iminoboronate-chitooligosaccharides hydrogels with strong antimicrobial activity for biomedical applications, *Carbohydr. Polym.*, 2022, **276**, 118727, DOI: **10.1016/j.carbpol.2021.118727**.

30 J. Lambert and T. A. Muir, *Practical chemistry*, Heineman, London, 3rd edn, 1973.

31 M. S. Arayne, N. Sultana and S. Begum, A new colorimetric method for the assay of erythromycin, *J. Pak. Med. Assoc.*, 1983, **33**, 256–259.

32 C. W. Chase, D. E. Barker, W. L. Russell and R. P. Burns, Serum amylase and lipase in the evaluation of acute abdominal pain, *Am. Surg.*, 1996, **62**, 1028–1033.

33 A. Hasmann, E. Wehrschuetz-Sigl, G. Kanzler, U. Gewessler, E. Hulla, K. P. Schneider, B. Binder, M. Schintler and G. M. Guebitz, Novel peptidoglycan-based diagnostic devices for detection of wound infection, *Diagn. Microbiol. Infect. Dis.*, 2011, **71**, 12–23, DOI: **10.1016/j.diagmicrobio.2010.09.009**.

34 A. W. Bauer, Single-Disk Antibiotic-Sensitivity Testing of Staphylococci, *AMA Arch. Intern. Med.*, 1959, **104**, 208–216, DOI: **10.1001/archinte.1959.00270080034004**.

35 B.-I. Andreica, A. Anisiei, I. Rosca, A.-I. Sandu, A. S. Pasca, L. M. Tartau and L. Marin, Quaternized chitosan/chitosan nanofibrous mats: An approach toward bioactive materials for tissue engineering and regenerative medicine, *Carbohydr. Polym.*, 2023, **302**, 120431, DOI: **10.1016/j.carbpol.2022.120431**.

36 ISO - ISO 10993-5:2009 - biological evaluation of medical devices—part 5: tests for *in vitro* cytotoxicity.

37 A. Moudgil and B. P. Chaudhari, Understanding Critical Aspects of Liposomal Synthesis for Designing the Next Generation Targeted Drug Delivery Vehicle, *ChemistrySelect*, 2023, **8**, e202302435, DOI: **10.1002/slct.202302435**.

38 F. Brunel, L. Véron, L. David, A. Domard and T. Delair, A Novel Synthesis of Chitosan Nanoparticles in Reverse

Emulsion, *Langmuir*, 2008, **24**, 11370–11377, DOI: **10.1021/la801917a**.

39 Y. Lo, J. Tsai and J. Kuo, Liposomes and disaccharides as carriers in spray-dried powder formulations of superoxide dismutase, *J. Controlled Release*, 2004, **94**, 259–272, DOI: **10.1016/j.jconrel.2003.09.019**.

40 H. Nsairat, D. Khater, U. Sayed, F. Odeh, A. Al Bawab and W. Alshaer, Liposomes: structure, composition, types, and clinical applications, *Heliyon*, 2022, **8**, e09394, DOI: **10.1016/j.heliyon.2022.e09394**.

41 K. Djanashvili, T. L. M. ten Hagen, R. Blangé, D. Schipper, J. A. Peters and G. A. Koning, Development of a liposomal delivery system for temperature-triggered release of a tumor targeting agent, Ln(III)-DOTA-phenylboronate, *Bioorg. Med. Chem.*, 2011, **19**, 1123–1130, DOI: **10.1016/j.bmc.2010.06.036**.

42 J. M. Abu Ershaid, S. M. Abudoleh and D. N. Lafi, Freeze-dried erythromycin nanocrystals: preparation, characterisation, antimicrobial activity, and aerodynamic properties, *Pharmacia*, 2024, **71**, 1–10, DOI: **10.3897/pharmacia.71.e127826**.

43 N. Forna, D. Damir, L. D. Duceac, M. G. Dabija, G. Calin, D. L. Ichim, C. Gutu, C. Grierosu, L. Eva, M. I. Ciuhodaru, E. R. B. Goroftei, E. A. Banu, L. Stafie, C. Gabriela, G. Mitrea and C. Marcu, Nano-Architectonics of Antibiotic-Loaded Polymer Particles as Vehicles for Active Molecules, *Appl. Sci.*, 2022, **12**, 1998, DOI: **10.3390/app12041998**.

44 R. S. Nair, N. Billa, L. Y. Mooi and A. P. Morris, Characterization and *ex vivo* evaluation of curcumin nanoethosomes for melanoma treatment, *Pharm. Dev. Technol.*, 2022, **27**, 72–82, DOI: **10.1080/10837450.2021.2023568**.

45 V. Mohan, C. D. Naske, C. N. Britten, L. Karimi and K. B. Walters, Hydroxide-catalyzed cleavage of selective ester bonds in phosphatidylcholine: An FTIR study, *Vib. Spectrosc.*, 2020, **109**, 103055, DOI: **10.1016/j.vibspec.2020.103055**.

46 I. S. Ryu, X. Liu, Y. Jin, J. Sun and Y. J. Lee, Stoichiometric analysis of competing intermolecular hydrogen bonds using infrared spectroscopy, *RSC Adv.*, 2018, **8**, 23481–23488, DOI: **10.1039/C8RA02919A**.

47 J. R. Everett and J. W. Tyler, An analysis of the 1H and 13C n.m.r. spectra of erythromycin a using two-dimensional methods, *J. Chem. Soc., Perkin Trans. 1*, 1985, 2599, DOI: **10.1039/p19850002599**.

48 A. Timoszyk and L. Latanowicz, Interactions of sialic acid with phosphatidylcholine liposomes studied by 2D NMR spectroscopy, *Acta Biochim. Pol.*, 2013, **60**, 539–546, DOI: **10.18388/abp.2013_2018**.

49 X.-R. Shao, X.-Q. Wei, S. Zhang, N. Fu, Y.-F. Lin, X.-X. Cai and Q. Peng, Effects of Micro-environmental pH of Liposome on Chemical Stability of Loaded Drug, *Nanoscale Res. Lett.*, 2017, **12**, 504, DOI: **10.1186/s11671-017-2256-9**.

50 S. Ong, L. Ming, K. Lee and K. Yuen, Influence of the Encapsulation Efficiency and Size of Liposome on the Oral Bioavailability of Griseofulvin-Loaded Liposomes, *Pharmaceutics*, 2016, **8**, 25, DOI: **10.3390/pharmaceutics8030025**.

51 N. A. Ramli, N. Ali, S. Hamzah and N. I. Yatim, Physicochemical characteristics of liposome encapsulation of stingless bees' propolis, *Heliyon*, 2021, **7**, e06649, DOI: **10.1016/j.heliyon.2021.e06649**.

52 R. Censi and P. D. Martino, Polymorph Impact on the Bioavailability and Stability of Poorly Soluble Drugs, *Molecules*, 2015, **20**, 18759–18776, DOI: **10.3390/molecules201018759**.

53 C. Nunes, A. Mahendrasingam and R. Suryanarayanan, Quantification of Crystallinity in Substantially Amorphous Materials by Synchrotron X-ray Powder Diffractometry, *Pharm. Res.*, 2005, **22**, 1942–1953, DOI: **10.1007/s11095-005-7626-9**.

54 K. Fujii, M. Aoki and H. Uekusa, Solid-State Hydration/Dehydration of Erythromycin A Investigated by ab Initio Powder X-ray Diffraction Analysis: Stoichiometric and Nonstoichiometric Dehydrated Hydrate, *Cryst. Growth Des.*, 2013, **13**, 2060–2066, DOI: **10.1021/cg400121u**.

55 P. M. Matei, P. Martín-Ramos, M. Sánchez-Báscones, S. Hernández-Navarro, A. Correa-Guimaraes, L. M. Navas-Gracia, C. A. Rufino, M. C. Ramos-Sánchez and J. Martín-Gil, Synthesis of Chitosan Oligomers/Propolis/Silver Nanoparticles Composite Systems and Study of Their Activity against *Diplodia seriata*, *Int. J. Polym. Sci.*, 2015, **2015**, 1–11, DOI: **10.1155/2015/864729**.

56 J. T. Carstensen and K. Van Scoik, Amorphous-to-Crystalline Transformation of Sucrose, *Pharm. Res.*, 1990, **07**, 1278–1281, DOI: **10.1023/A:1015942022789**.

57 L. Deng, Y. Wang, H. Jiang, X. Xu, J. Han and W. Liu, Specific protection mechanism of oligosaccharides on liposomes during freeze-drying, *Food Res. Int.*, 2023, **166**, 112608, DOI: **10.1016/j.foodres.2023.112608**.

58 R. Pignatello, P. Simerska, A. Leonardi, A. S. Abdelrahim, G. P. Petronio, V. Fuochi, P. M. Furneri, B. Ruozi and I. Toth, Synthesis, characterization and in vitro evaluation of amphiphilic ion pairs of erythromycin and kanamycin antibiotics with liposaccharides, *Eur. J. Med. Chem.*, 2016, **120**, 329–337, DOI: **10.1016/j.ejmech.2016.04.074**.

59 M. N. Najafi, A. Arianmehr and A. M. Sani, Preparation of Barije (Ferula gummosa) Essential Oil–Loaded Liposomes and Evaluation of Physical and Antibacterial Effect on Escherichia coli O157:H7, *J. Food Prot.*, 2020, **83**, 511–517, DOI: **10.4315/0362-028X.JFP-19-285**.

60 P. da S. Malheiros, V. Sant'Anna, M. de, S. Barbosa, A. Brandelli and B. D. G. de M. Franco, Effect of liposome-encapsulated nisin and bacteriocin-like substance P34 on Listeria monocytogenes growth in Minas frescal cheese, *Int. J. Food Microbiol.*, 2012, **156**, 272–277, DOI: **10.1016/j.ijfoodmicro.2012.04.004**.

61 C. V. Rimoli, R. de Oliveira Pedro and P. B. Miranda, Interaction mechanism of chitosan oligomers in pure water with cell membrane models studied by SFG

vibrational spectroscopy, *Colloids Surf., B*, 2022, **219**, 112782, DOI: **10.1016/j.colsurfb.2022.112782**.

62 V. Nagy, S. Quader and M. Másson, Fine-tuning the cytotoxicity profile of N,N,N-trimethyl chitosan through trimethylation, molecular weight, and polyelectrolyte complex nanoparticles, *Int. J. Biol. Macromol.*, 2024, **281**, 135805, DOI: **10.1016/j.ijbiomac.2024.135805**.

63 T. M. Ways, W. Lau and V. Khutoryanskiy, Chitosan and Its Derivatives for Application in Mucoadhesive Drug Delivery Systems, *Polymers*, 2018, **10**, 267, DOI: **10.3390/polym10030267**.

64 W. E. Vargas, Refractive indices of chitin, chitosan, and uric acid with application to structural color analysis, *Opt. Pura Apl.*, 2013, **46**, 55–72, DOI: **10.7149/OPA.46.1.55**.

65 M. Ardhammar, P. Lincoln and B. Nordén, Invisible liposomes: Refractive index matching with sucrose enables flow dichroism assessment of peptide orientation in lipid vesicle membrane, *Proc. Natl. Acad. Sci. U. S. A.*, 2002, **99**, 15313–15317, DOI: **10.1073/pnas.192583499**.

66 F. M. Goycoolea, G. Lollo, C. Remuñán-López, F. Quaglia and M. J. Alonso, Chitosan-Alginate Blended Nanoparticles as Carriers for the Transmucosal Delivery of Macromolecules, *Biomacromolecules*, 2009, **10**, 1736–1743, DOI: **10.1021/bm9001377**.

67 I. A. Sogias, A. C. Williams and V. V. Khutoryanskiy, Why is Chitosan Mucoadhesive?, *Biomacromolecules*, 2008, **9**, 1837–1842, DOI: **10.1021/bm800276d**.

68 F. Amadei, B. Fröhlich, W. Stremmel and M. Tanaka, Nonclassical Interactions of Phosphatidylcholine with Mucin Protect Intestinal Surfaces: A Microinterferometry Study, *Langmuir*, 2018, **34**, 14046–14057, DOI: **10.1021/acs.langmuir.8b03035**.

69 A. A. H. Al Qushawi and K. J. Al-Ruaby, Antibacterial Activity Study of Erythromycin-Loaded Chitosan Nanoparticles and Chitosan Nanoparticle against Identified MRSA and MSSA Bacteria Isolated from Mastitis Cow Milk, *EurAsian J. BioSci.*, 2020, **14**, 7397–7405.

70 V. T. Perchyonok, S. Zhang, N. Basson, S. R. Grobler, T. G. Oberholzer and M. Ward, Insights into Functional Erythromycin/Antioxidant Containing Chitosan Hydrogels as Potential Bio-active Restorative Materials: Structure, Function and Antimicrobial Activity, *Adv. Tech. Biol. Med.*, 2014, **2**, 10001156, DOI: **10.4172/2379-1764.1000116**.

71 T. Sun, D. Zhou, J. Xie and F. Mao, Preparation of chitosan oligomers and their antioxidant activity, *Eur. Food Res. Technol.*, 2007, **225**, 451–456, DOI: **10.1007/s00217-006-0439-1**.

72 Y. Xiaofei, L. Tingting, W. Xuan and H. Zhiyi, Erythromycin attenuates oxidative stress-induced cellular senescence via the PI3K-mTOR signaling pathway in chronic obstructive pulmonary disease, *Front. Pharmacol.*, 2022, **13**, 1043474, DOI: **10.3389/fphar.2022.1043474**.

73 H. Saito and K. Ishihara, Antioxidant activity and active sites of phospholipids as antioxidants, *J. Am. Oil Chem. Soc.*, 1997, **74**, 1531–1536, DOI: **10.1007/s11746-997-0072-6**.

74 S. S. Elblehi, M. H. Hafez and Y. S. El-Sayed, L-α-Phosphatidylcholine attenuates mercury-induced hepato-renal damage through suppressing oxidative stress and inflammation, *Environ. Sci. Pollut. Res.*, 2019, **26**, 9333–9342, DOI: **10.1007/s11356-019-04395-9**.

75 T. Maliar, M. Blažková, J. Polák, M. Maliarová, E. Ürgeová and J. Viskupičová, Antioxidant and Pro-Oxidant Properties of Selected Clinically Applied Antibiotics: Therapeutic Insights, *Pharmaceuticals*, 2024, **17**, 1257, DOI: **10.3390/ph17101257**.

76 J. A. Washington and W. R. Wilson, Erythromycin: A Microbial and Clinical Perspective After 30 Years of Clinical Use (First of Two Parts), *Mayo Clin. Proc.*, 1985, **60**, 189–203, DOI: **10.1016/S0025-6196(12)60219-5**.

77 M. Nasaj, M. Chehelgerdi, B. Asghari, A. Ahmadieh-Yazdi, M. Asgari, S. Kabiri-Samani, E. Sharifi and M. Arabestani, Factors influencing the antimicrobial mechanism of chitosan action and its derivatives: A review, *Int. J. Biol. Macromol.*, 2024, **277**, 134321, DOI: **10.1016/j.ijbiomac.2024.134321**.

78 S. Ramadan, S. N. Tammam, M. A. S. Boushehri, H.-G. Breitinger, U. Breitinger, S. Mansour and A. Lamprecht, Liposomal delivery of functional transmembrane ion channels into the cell membranes of target cells; a potential approach for the treatment of channelopathies, *Int. J. Biol. Macromol.*, 2020, **153**, 1080–1089, DOI: **10.1016/j.ijbiomac.2019.10.238**.

79 J.-H. Liang and X. Han, Structure-Activity Relationships and Mechanism of Action of Macrolides Derived from Erythromycin as Antibacterial Agents, *Curr. Top. Med. Chem.*, 2013, **13**, 3131–3164, DOI: **10.2174/15680266113136660223**.

80 S. S. Sana, R. Vadde, S. Atapakala, M. M. Alam, N. Mamidi and S.-C. Kim, An eco-friendly lignin sulfonate-stabilized ZnO nanoflowers with inherent antioxidant, antibacterial, anticancer activities and effect on seed germination, *Int. J. Biol. Macromol.*, 2025, **313**, 144089, DOI: **10.1016/j.ijbiomac.2025.144089**.

81 S. Battista, P. Bellio, L. Fagnani, E. Allegritti, L. Nazzicone, L. Galantini, G. Celenza and L. Giansanti, Structurally Related Liposomes Containing *N*-Oxide Surfactants: Physicochemical Properties and Evaluation of Antimicrobial Activity in Combination with Therapeutically Available Antibiotics, *Mol. Pharm.*, 2022, **19**, 788–797, DOI: **10.1021/acs.molpharmaceut.1c00609**.

82 C. Mugabe, A. O. Azghani and A. Omri, Preparation and characterization of dehydration–rehydration vesicles loaded with aminoglycoside and macrolide antibiotics, *Int. J. Pharm.*, 2006, **307**, 244–250, DOI: **10.1016/j.ijpharm.2005.10.005**.

83 B. M. Salah, M. Rady, M. Abdel-Halim, H. M. Fahmy, N. S. El-Din and M. H. Gaber, Alternating Magnetic Field Induced Membrane Permeability in Erythromycin Magneto-Liposomes A Potential Solution to Antibiotic

Resistance, *Biophysics*, 2021, **66**, 264–272, DOI: **10.1134/S0006350921020196**.

84 B. Godin and E. Touitou, Erythromycin Ethosomal Systems: Physicochemical Characterization and Enhanced Antibacterial Activity, *Curr. Drug Delivery*, 2005, **2**, 269–275, DOI: **10.2174/1567201054367931**.

85 A. Valizadeh, M. H. Darvishi, A. Amani and A. A. K. Zarchi, Design and development of novel formulation of Aloe Vera nanoemulsion gel contained erythromycin for topical antibacterial therapy: In vitro and in vivo assessment, *J. Drug Delivery Sci. Technol.*, 2022, **74**, 103519, DOI: **10.1016/j.jddst.2022.103519**.

86 V. M. Platon, B. I. Andreica, A. Anisiei, I. Rosca, I. A. Sandu, L. Mititelu Tartau and L. Marin, Antioxidant-sealed chitosan nanofibers loaded with erythromycin: Tissue regeneration biomaterials with immune-modulating effects in a rat model, *Carbohydr. Polym.*, 2025, **368**, 124247, DOI: **10.1016/j.carbpol.2025.124247**.

87 S. Fathollahipour, A. Abouei Mehrizi, A. Ghaee and M. Koosha, Electrospinning of PVA/chitosan nanocomposite nanofibers containing gelatin nanoparticles as a dual drug delivery system, *J. Biomed. Mater. Res., Part A*, 2015, **103**, 3852–3862, DOI: **10.1002/jbm.a.35529**.

88 H. Park, H. Park and K. Na, Dual *Propionibacterium acnes* therapy using skin penetration-enhanced liposomes loaded with a photosensitizer and an antibiotic, *J. Porphyrins Phthalocyanines*, 2015, **19**, 956–966, DOI: **10.1142/S1088424615500686**.

89 K. Mayattu, J. Rajwade and V. Ghormade, Development of erythromycin loaded PLGA nanoparticles for improved drug efficacy and sustained release against bacterial infections and biofilm formation, *Microb. Pathog.*, 2024, **197**, 107083, DOI: **10.1016/j.micpath.2024.107083**.

90 T. Liu, T. Wu, H. Liu, B. Ke, H. Huang, Z. Jiang and M. Xie, Ultraviolet–crosslinked hydrogel sustained–release hydrophobic antibiotics with long–term antibacterial activity and limited cytotoxicity, *J. Appl. Polym. Sci.*, 2014, **131**, 40438, DOI: **10.1002/app.40438**.

91 L. T. C. Tran, C. Gueutin, G. Frebourg, C. Burucoa and V. Faivre, Erythromycin encapsulation in nanoemulsion-based delivery systems for treatment of Helicobacter pylori infection: Protection and synergy, *Biochem. Biophys. Res. Commun.*, 2017, **493**, 146–151, DOI: **10.1016/j.bbrc.2017.09.060**.

92 E. Marian, M. Muresan, T. Jurca and L. Vicas, Evaluation of antimicrobial activity of some types of inclusion complexes of erythromycin with β-cyclodextrin on Staphylococcus aureus, *Farmacia*, 2013, **61**, 518–525.

93 F. Wu, H. Zheng, W. Wang, Q. Wu, Q. Zhang, J. Guo, B. Pu, X. Shi, J. Li, X. Chen and W. Hong, Rapid eradication of antibiotic-resistant bacteria and biofilms by MXene and near-infrared light through photothermal ablation, *Sci. China Mater.*, 2021, **64**, 748–758, DOI: **10.1007/s40843-020-1451-7**.

94 A. Dunai, R. Spohn, Z. Farkas, V. Lázár, Á. Györkei, G. Apjok, G. Boross, B. Szappanos, G. Grézal, A. Faragó, L. Bodai, B. Papp and C. Pál, Rapid decline of bacterial drug-resistance in an antibiotic-free environment through phenotypic reversion, *eLife*, 2019, **8**, e47088, DOI: **10.7554/eLife.47088**.

95 J. M. Blondeau, L. D. Blondeau and S. D. Fitch, In vitro killing of drug susceptible and multidrug resistant bacteria by amikacin considering pulmonary drug concentrations based on an inhaled formulation, *J. Chemother.*, 2024, **36**, 389–397, DOI: **10.1080/1120009X.2024.2313908**.

96 M. Millrose, M. Kruse, B. Flick and R. Stahlmann, Effects of macrolides on proinflammatory epitops on endothelial cells in vitro, *Arch. Toxicol.*, 2009, **83**, 469–476, DOI: **10.1007/s00204-008-0388-5**.

97 M. Kruse, B. Kilic, B. Flick and R. Stahlmann, Effect of quinupristin/dalfopristin on 3T3 and Eahy926 cells in vitro in comparison to other antimicrobial agents with the potential to induce infusion phlebitis, *Arch. Toxicol.*, 2007, **81**, 447–452, DOI: **10.1007/s00204-006-0163-4**.

98 M. Płaczek, D. Wątróbska-Świetlikowska, J. Stefanowicz-Hajduk, M. Drechsler, J. R. Ochocka and M. Sznitowska, Comparison of the in vitro cytotoxicity among phospholipid-based parenteral drug delivery systems: Emulsions, liposomes and aqueous lecithin dispersions (WLDs), *Eur. J. Pharm. Sci.*, 2019, **127**, 92–101, DOI: **10.1016/j.ejps.2018.10.018**.

99 R. P. Singh, H. V. Gangadharappa and K. Mruthunjaya, Phospholipids: Unique carriers for drug delivery systems, *J. Drug Delivery Sci. Technol.*, 2017, **39**, 166–179, DOI: **10.1016/j.jddst.2017.03.027**.

100 N. A. M. Nor, A. S. Halim, S. Shamsuddin, C. M. C. Hussin, Z. Ujang and A. H. A. Rashid, The effect of chitosan derivatives film on the proliferation of human skin fibroblasts: An in vitro study, *J. Sustainability Sci. Manage.*, 2013, **8**, 212–219.

101 M. S. B. A. Rasad, A. S. Halim, K. Hashim, A. H. A. Rashid, N. Yusof and S. Shamsuddin, In vitro evaluation of novel chitosan derivatives sheet and paste cytocompatibility on human dermal fibroblasts, *Carbohydr. Polym.*, 2010, **79**, 1094–1100, DOI: **10.1016/j.carbpol.2009.10.048**.

102 A. K. F. Dyab, M. A. Mohamed, N. M. Meligi and S. K. Mohamed, Encapsulation of erythromycin and bacitracin antibiotics into natural sporopollenin microcapsules: antibacterial, cytotoxicity, *in vitro* and *in vivo* release studies for enhanced bioavailability, *RSC Adv.*, 2018, **8**, 33432–33444, DOI: **10.1039/C8RA05499A**.

103 M. Doostan, H. Maleki, M. Doostan, K. Khoshnevisan, R. Faridi-Majidi and E. Arkan, Effective antibacterial electrospun cellulose acetate nanofibrous patches containing chitosan/erythromycin nanoparticles, *Int. J. Biol.*

Macromol., 2021, **168**, 464–473, DOI: **10.1016/j. ijbiomac.2020.11.174**.

104 Z. Rukavina, M. Š Klarić, J. Filipović-Grčić, J. Lovrić and Ž Vanić, Azithromycin-loaded liposomes for enhanced topical treatment of methicillin-resistant Staphyloccocus aureus (MRSA) infections, *Int. J. Pharm.*, 2018, **553**, 109–119, DOI: **10.1016/j. ijpharm.2018.10.024**.